Deformations of ship sections during fabrication, causes and remedies

Auteur : Eisawy, Mohamed
Promoteur(s) : 14956
Faculté : Faculté des Sciences appliquées
Diplôme : Master : ingénieur civil mécanicien, à finalité spécialisée en "Advanced Ship Design"
Année académique : 2020-2021
URI/URL : http://hdl.handle.net/2268.2/13647

Deformations on the Ship Sections During Fabrication: Cause and Remedies

Submitted on 05 September 2021

by

EISAWY Mohamed | Str. Parcului nr. 4| 800201 Galati. |

mohamed.3isawy@gmail.com

Student ID No.: 220202362

First Reviewer:

Prof. Dr Patrick Kaeding

Pro-Rector of Studying, Teaching and Evaluation (PSL)

University of Rostock

Universitätsplatz 1

18055, Rostock

Germany

Second Reviewer:

Prof. Renardo-Florin Teodor

Associate Professor

Dunarea de Jos University
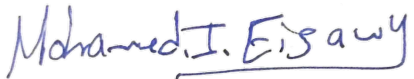
47, Domneasca Street

800008, Galati

Romania

EMship+
Advanced Design

Master Thesis

ACKNOWLEDGEMENTS

EISAWY Mohamed

DECLARATION OF AUTHORSHIP

I, EISAWY Mohamed, declare that this thesis and the work presented in it are my own and have been generated by me as the result of my own original research.

Where I have consulted the published work of others, this is always clearly attributed.

Where I have quoted from the work of others, the source is always given. With the exception of such quotations, this thesis is entirely my own work.

I have acknowledged all main sources of help.

Where the thesis is based on work done by myself jointly with others, I have made clear exactly what was done by others and what I have contributed myself.

This thesis contains no material that has been submitted previously, in whole or in part, for the award of any other academic degree or diploma.

I cede copyright of the thesis in favour of the University of Rostock

Date: Signature
06/09/2021

TABLE OF CONTENTS

ABBREVIATIONS

FEM	*Finite element method*
δh	*Reduction in height caused by the cumulative effect of shrinkage*
δB	*Reduction in breadth due to cumulative effect of shrinkage*
B	*Breadth of the ship section*
γ_f	*Fine mesh yield utilization factor*
σ_{vm}	*Von Mises sress, in N/mm^2*
σ_{axial}	*Axial sress in rod element, in N/mm^2*
σ_{fperm}	*Permissible fine mesh utilization factor*
R_Y	*Nominal yield stress, taken equal to $235/k$ N/mm^2*
AC	*Aceptance criteria*
COG	*Center of gravity*
DAF	*Dynamic amplification factor*

LIST OF FIGURES

LIST OF TABLES

ABSTRACT

During fabrication process, material deformations are likely to occur due to various factors such as heat during steel cutting, welding induced deformations, lifting and turning of ship sections, temporary stiffening and other possible modifications of ship sections. Lifting induced deformations is one of the major causes of deformations that highly affect the production cost and quality. The aim of this thesis is to outline the main causes of deformations that occur in ship sections during fabrication and to analyse in detail the lifting and turning operations of one ship section using the Finite Element Method (FEM). A strength check using the FEM has been performed on the selected ship section to investigate the deformations and stresses in two different cases with three different loading conditions. First, the section has been analysed without temporary stiffening in three load scenarios: lifting before turning, worst-case scenario during turning and lifting after turning. Similarly, the second case study has been analysed but with the temporary stiffening added according to the lifting plan. Various influencing parameters that determine the lifting plan has been investigated such as the sling angle which directly affects the deformation characteristics. It is observed that the addition of temporary stiffening is essential to minimize the deformations and to maintain the stress levels below the yield point.

1 INTRODUCTION

The shipbuilding process is guided by three main targets: quality, cost, and construction time. If the quality of the ship is high and the construction cost is low as well as the delivery time is not exceeded, the two parties involved in the contract (client and shipyard) will be satisfied. Thus, a good reputation of the shipyard is achieved and more new ship orders are expected to be placed.

During fabrication processes, material deformations are likely to occur due to various factors such as heat during steel cutting, welding induced deformations (longitudinal shrinkage, transverse shrinkage, longitudinal deflection, and angular distortion), transport and turning of the ship sections, temporary stiffening of ship sections during fabrication and modifications of ship sections.

A ship block is formed by assembling two or more ship sections. While a ship section is formed by assembling prefabricated steel panels. The dimensions accuracy of each fabricated steel panel is essential for the overall dimensions accuracy of the ship section. Welding deformations result in inadequate appearance and poor quality. For example, welding induced shrinkage can cause a mismatch in the dimensions of the steel panels posing significant challenges in the structural fit and placement. An appropriate shrinkage allowance should be used to minimize the shrinkage during the fabrication stage. The combined effect of distortion and shrinkage caused by the welding process during the fabrication of ship hull sections results in an overall change in dimensions(Mandal, 2017). The cumulative effect of shrinkage causes a reduction in the height and breadth of the ship sections as shown in Fig.1.
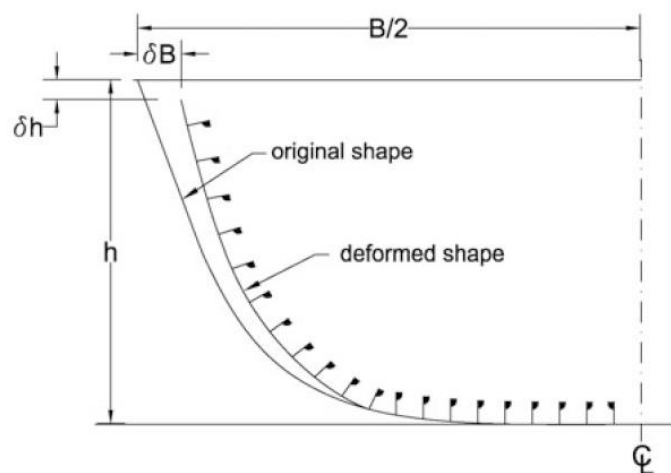
Figure 1 Shrinkage of ship section (Mandal, 2017).

In modern shipbuilding, the division of ship sections tends to be large, and the structure tends to become more complicated. Moreover, the difficulty of lifting increases accordingly. The rationality and feasibility of a lifting plan directly determine if the lifting work can be carried out safely and efficiently (Li Rui et al., 2013).

During the construction phase, the lifting accidents can be catastrophic leading to injury/ loss of lives. In addition, it can cause severe damage to the ship section and the surrounding structures. The deformation removal requires additional work which increases the overall production cost and construction time. At the construction site, when joining the ship sections together, the deformations mitigation is needed to minimize the production cost and time(Samin. CO, 2013)

The ship section lifting plan is developed based on the actual situation of the current shipyard lifting capabilities. The purpose is to provide an intelligent and effective procedure, which can speed up the lifting design process.

The lifting plan design is generally carried out starting by the determination of the position of the lifting lugs according to the weight, centre of gravity and structural characteristics of the ship section, combined with the specifications of the lifting site and lifting equipment. Then, select the appropriate lifting lug and sling specifications. After that, a strength check should be performed to find out whether the section needs temporary stiffening.

The lifting plan design should meet the principles of safety and rationality(Li Rui et al., 2013). The principle of safety includes:

- The lifting process should always maintain a stable state,
- The weight to be lifted is less than the maximum rated load of the crane,
- The load of a single hook is less than its maximum rated load,
- The load of a single lifting lug is less than its specification load,
- The strength of the plate where the lifting lug is welded must be large enough,
- The low-strength parts should be reinforced with temporary stiffeners.

The principle of rationality includes:

- The lifting points are evenly and reasonably distributed around the centre of gravity to avoid any serious motions,
- The lifting points should be set on strong members as much as possible,
- The distance between the lifting points is reasonably arranged to meet the crane specifications,
- The positions of the lifting lugs should be convenient for assembly and welding.

The material deformations lead to a mismatch of the hull interior and exterior plating as well as the outfitting such as the various types of pipes. However, in order to easily assemble the sections to form the block, the misalignments can be avoided by having not extremely stiff ship sections.

Before lifting, the correct arrangement of the cables and shackles should be checked with the utmost care. The section will be raised 50 mm above the ground, remaining in this position for 15 minutes, during which time the section will be inspected for deformations, detachments or other aspects that appear that would endanger the lifting operation. After ensuring that there are no problems, the lifting/transport operation will continue(Damen Shipyards Galati report, n.d.).

All the lifting and turning operations must be performed by trained personnel capable of executing them in the presence of the team leader. Only authorized welders shall weld the lifting lugs. After visually checking the welding, the foreman calls the non-destructive test (NDT) team to perform the specific checks. If required, the defective welding is repaired. No lifting operations shall be made unless the NDT team confirmed that the lugs welding is good. After mounting the section, all the consolidations mounted according to this plan will be removed where necessary(Damen Shipyards Galati report, n.d.).

2 LITERATURE REVIEW

Many researchers have used the finite element method in order to predict the welding induced imperfections such as distortion and residual stresses. Furthermore, different parameters such as welding sequence, heat input, and welding speed were investigated to mitigate the welding deformations as these parameters are of great importance from the design perspective.

A three-dimensional thermo-elastic-plastic finite element method has been used by (Yi et al., 2020) to predict the welding induced imperfections of a full-scale stiffened panel. Validation of the numerical results comparing to the direct measurements using a 3D scanner has been accomplished and the results were consistent. It is concluded that the 3D scanner can measure the initial deformations effectively.

(Wang et al., 2018) and (Wang et al., 2016) proposed a computational approach based on inherent deformation for predicting welding deformations and described its framework and application. Based on computational results, the welding inherent deformation was assessed; an elastic FE analysis with welding inherent deformations as input parameters was used to predict out-of-plane welding distortion and critical welding buckling conditions. Also, the intermittent welding technique was used to minimize welding inherent deformation and sequentially avoid welding induced buckling. It is concluded that the intermittent zig-zag welding produces less in-plane inherent deformation and does not produce welding induced buckling, but it does not produce out-of-plane welding distortion.

Thermal elastic-plastic FE analysis has been used by (Wang et al., 2013) based on the inherent deformation theory to predict and mitigate the out-of-plane distortion in steel panels. The line heating method was used to mitigate the out-of-plane distortion. To correct buckling distortion, the in-plane inherent strain produced by line heating is introduced to the model edge. It is concluded that welding distortion can be reduced by using line heating to remove angular distortion.

(Hammad, Churiaque, et al., 2021) recently established a three-dimensional coupled thermo-elastic-plastic FE model in ABAQUS to simulate the volumetric heat flux distributions of the Hybrid Laser Arc Welding HLAW process. The FE model is validated by comparing its results with the experimental measurements. The effect of changing the welding sequence on the semi-industrial scale stiffened panel has also been investigated. Changing the welding sequence has

a serious influence on the vertical deflection distribution and magnitude, according to the research results.

A numerical simulation based on FE modelling to investigate the effect of geometrical properties and welding sequence on the magnitude of welding imperfections in a fabricated T-girder is established by (Hammad, Abdel-Nasser, et al., 2021). The out-of-plane distortion is reduced when the geometrical properties of a fabricated T-girder are modified without changing the required section modulus. Furthermore, using the non-continuous welding sequence highly reduced the out-of-plane distortion.

(Batista, 2012) has used the statistical software Design-Expert to predict welding deformations in thin plate panels. The experimental data from the trial in the shipyard was consistent with predicted numerical results. Based on the inherent strain theory and the finite element method, (Jang et al., 2002) proposed an efficient method for predicting the weld deformation of complicated structures. The applicability of this method to simple ship hull blocks was confirmed by simulation of a stiffened panel.

The impact of welding sequences on the magnitude and shape of distortion when welding multiple flat-bar stiffeners to a steel plate is investigated using a numerical simulation based on the finite element method (Azad et al., 2020). The impact of eight welding sequences on the magnitude and shape of plate distortion is studied. It is concluded that the welding sequence has a significant impact on the magnitude of deformation than residual stresses.

Researchers have also investigated the effect of lifting and turning operations on the deformation of the ship sections. (Galatanu et al., 2020) Adding temporary stiffeners had a significant influence on reducing the maximum stresses and deformations.

According to the number of equalizers, (Chun et al., 2018)three types of equations to find the block's initial equilibrium position. The experiments demonstrated that the proposed methods can be used to accurately determine the block's initial equilibrium position for block lifting.

(Lee et al., 2016) Analyzed the lifting and turning operations of ship block considering the force exerted on the block due to the contact with the slings. The Möller algorithm has been used to identify the contact, then the contact forces are determined by adding the tensions in the sling segments that include a contact point. It was concluded that that the contacts can be accurately checked, and the corresponding contact forces can be calculated.

3 FINITE ELEMENT METHOD

Finite element method is a systematic numerical technique used to approximately evaluate the structural behaviour when it's subjected to loads and constraints. Fig. 2 shows the workflow chart for performing the general FEA procedure. The main concept is to discretize the structure into a finite number of small elements that are connected at nodes. In the linear static problem, the equilibrium can be satisfied over the finite number of elements. Several different element shapes can be used, triangular and quadrilateral elements are typically used to model thin surfaces.

The stiffness matrix is then defined for each element. And based on the element connectivity, the element stiffness matrices are assembled into a global stiffness matrix. The global stiffness matrix will define how the structure will respond to the applied loads. It can be used along with the boundary conditions to solve for the displacement at each node in the structure. Once we have the displacements, we can calculate stresses, strains, and other field variables of interest.

The next step is postprocessing to obtain the desired results and validation of the model. The engineer is responsible for making sure that the problem has been properly defined, the mesh is suitable and connected, and is responsible for the analysis and interpretation of the results.

In general, structures have nonlinear behaviour especially when they are under loading because the stiffness of the structure changes after loading them. The system can be solved linearly if the structure has small deformations, the material has elastic behaviour, or the boundary conditions do not change with respect to time.

The section under this study is a linear static problem with small deformations, which means that the deformed section to the first order is identical to the undeformed one. If the yield point of the material is exceeded, the nonlinear FE analysis should be performed. Also, the user should evaluate the structural safety based on the analysis results along with the engineering knowledge and experience.

```
┌─────────────────────────────────┐
│        Select FEA Solver        │
│      SIMCENTER NASTRAN          │
└─────────────────────────────────┘
```

```
┌─────────────────────────────────┐
│ Pre-processing (Structural      │
│ Modelling)                      │          Check
│   • Create model geometry       │
│   • Define material properties  │
│   • Apply mesh pattern          │
│   • Apply boundary conditions   │
└─────────────────────────────────┘
```

```
┌─────────────────────────────────┐
│            Solution             │
│   • Assign analysis mode        │
│ (linear: small deflection)      │          Check
│   • Define calculation method   │
│ (linear: static general)        │
│   • Solve (Perform linear FEA)  │
└─────────────────────────────────┘
```

```
        ◇ Convergenc
          eachieved? ◇                    No
```

Yes

```
┌─────────────────────────────────┐
│      Post-processing results    │
│   • Stresses                    │
│   • Deformations                │
└─────────────────────────────────┘
```
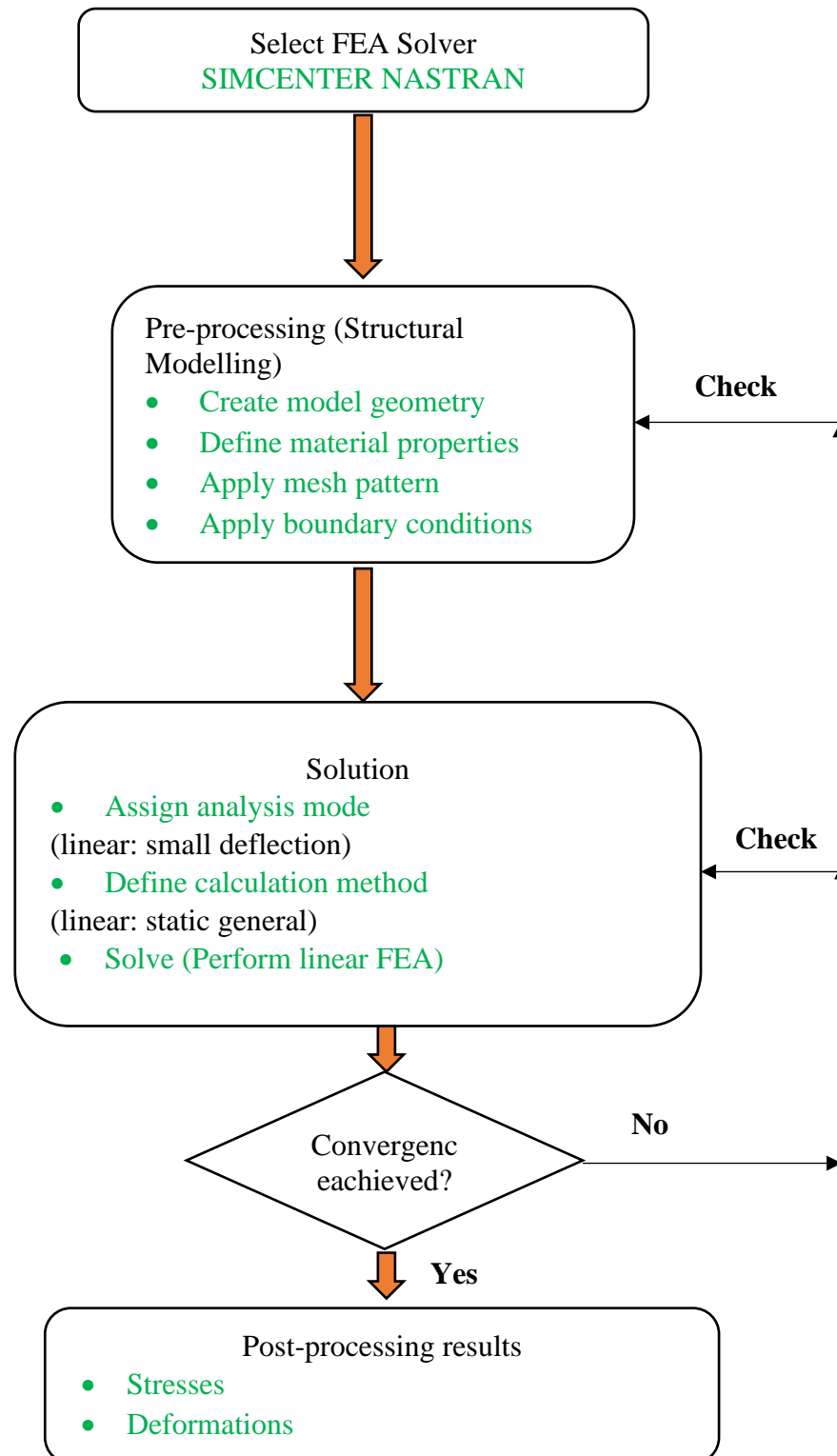
Figure 2 Workflow chart for performing general FEA procedure *(Alsayed & Ismail, 2019)*

4   METHODOLOGY

In this study, two cases have been studied. First, the section has been analysed without temporary stiffening in three load scenarios: lifting before turning, worst-case scenario during turning and lifting after turning. Similarly, the second case study has been analysed but with the temporary stiffening added according to the lifting plan

Before running the analysis, several checks have been done to ensure that the FE model is correctly set up such as checking the elements free edge, coincident nodes verify the mass of the structure to make sure that it meets the actual weight, running modal analysis to check and inspect possible deformation modes of the structure.

The lifting simulation was carried out using the Finite Element Method (FEM) to investigate the deformations that occur during the lifting process. The structural model was generated in Simcentre^{TM} FEMAP^{TM} (Finite Element Modelling and Postprocessing) and solved for a linear static stress analysis using Simcentre^{TM} Nastran^{TM} (NASA Structural Analysis). Both packages are provided by Siemens Digital Industries Software and have been extensively validated and widely recognized in the engineering simulation industry worldwide.

The model was created based on the 2D drawings of section 1172 taken from ROPAX Ferry. According to the lifting plan, temporary stiffeners were added to the model to compare the results of deformations and stress with the original model.

4.1   Structural Model

The selected section for this study was section number 1172 taken from a ROPAX Ferry. The section position is indicated in green in Fig.3, located in the forepart of the ferry and has an open structure at the aft part, while the fore part of the section has a transverse bulkhead which could lead to higher deformations in the aft part of the section.
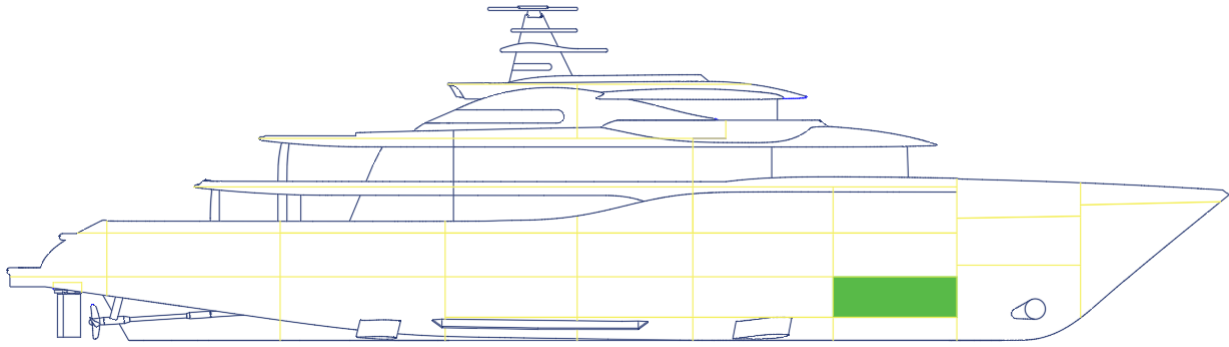
Figure 3 Ship section position (Lifting plan drawing).

Fig.4 shows isometric views of the section. The section different details are presented in appendicies19, 20, 21 and 22. It should be noted that the structural model has not been created or imported to the FEMAP. However, the different 2D views were utilized as a guide to directly create the FE model.
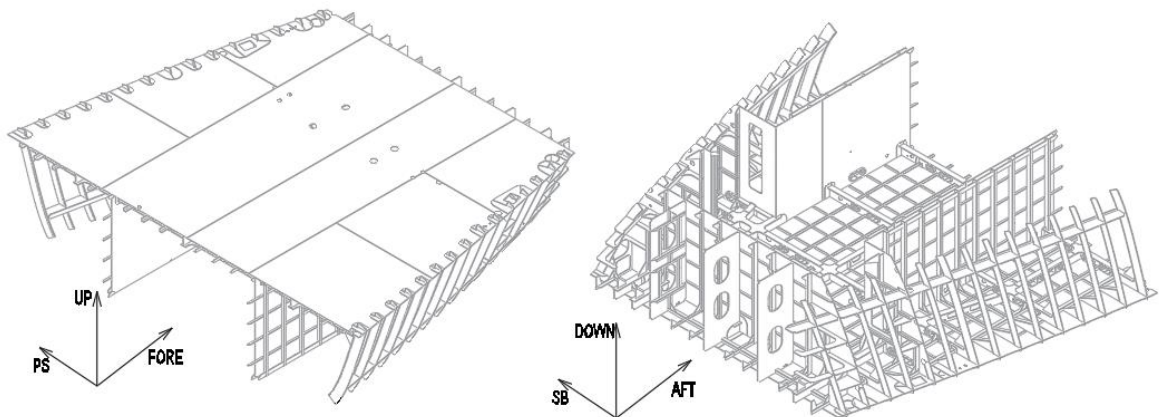
Figure 4 Isometric view of the section (Lifting plan drawing).

The FE model was simplified, i.e., scallops and welding seems have been ignored, brackets have been considered only in the area of interest in the hotspot regions and all the openings were approximately modelled. More care would be taken if the stress emerges around an opening.

4.2 Coordinate System

The FE coordinate system has been defined to be consistent with the naval architecture typical coordinate system. The X-axis is positive forward along the section length, the Y-axis is positive to the portside along with the section breadth and The Z-axis is positive upwards along with the section height.

4.3 Units

The units used to carry out the analysis for Inputs and outputs was newtons (N), millimeters (mm), ton per cubic millimeter (ton/mm^3) and Mega Pascal MPa (N/mm^2).

4.4 Materials

For a linear elastic static analysis, Young's Modulus and Poisson's Ratio are the essential parameters to be defined in the FEMAP (Ponthot, 2020). The material density has been added to apply the inertial load under gravitational acceleration. Table 1 summarizes the steel Mechanical properties as defined in the analysis set-up.

Table 1 Steel mechanical properties as defined in the FEA

(Https://Www.Makeitfrom.Com/Material-Properties/EN-1.0308-E235-Non-Alloy-Steel, 2020)

Item	Grade	Tensile Strength N/mm^2	Yield Strength N/mm^2	Young's Modulus N/mm^2	Poisson's Ratio
Hull section	A	420	235	206000	0.3
Lifting lugs	DH36	550	315	206000	0.3
Temporary stiffeners	E235	440	280	190000	0.29

4.5 Lifting Lugs

When lifting the ship section, two lifting lugs are usually installed at the fore and two at the aft of the section. Lifting lugs are welded to the section on positions according to the lifting plan. During the turning process, some lugs are to be burnt off to place the section in the right position without the existence of the undesired lugs. After welding the section to the adjacent one, the remaining lifting lugs are to be removed. The lifting lugs can be selected according to calculated load which must ensure safety and prevent waving of the lifted section(Li Rui et al., 2013). The lifting lugs are connected to the slings using shackles. Therefore, a consequence factor of 1.5

should be taken into account for the calculation of the lifting lug maximum load. Fig.5 shows the used lifting lugs according to the lifting plan.
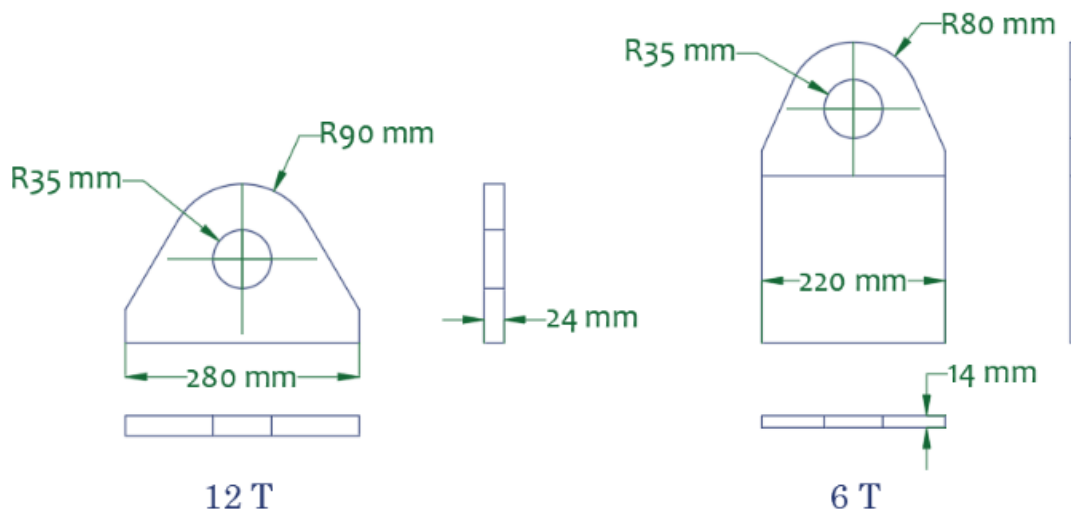

Figure 5 Lifting lugs according to the lifting plan (Lifting plan drawing).

4.6 Center of Gravity

Finite element analysis focuses on the structure components being analyzed. To accurately predict the structural behaviour, the section's mass needs to be corrected according to the actual weight estimation and centre of gravity (COG). Additional mass represents the steel outfitting (7 % of the section weight), and a safety coefficient (3 % of the total weight including the outfitting weight) was defined as a nonstructural mass in FEMAP to achieve the COG position. The approximate mass and COG have been taken from the lifting plan and summarized in Table 3. Welding seems and painting are considered by increasing the steel grade A density from 7.85 ton/m3 to 8.05 ton/m3 (Mirel Balan, Structural expert). The zero point and COG positions are shown in Fig.6.
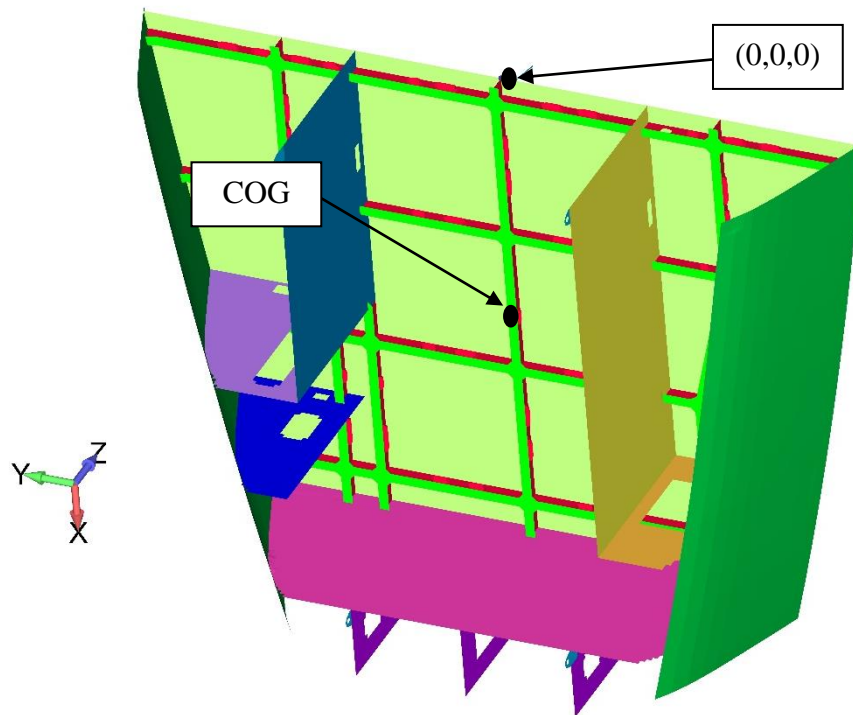
Figure 6 Zero point and center of gravity positions

Table 2 Mass and center of gravity (Lifting plan drawing).

Center of gravity (mm)		
X from (0,0,0)	**Y from (0,0,0)**	**Z from (0,0,0)**
3899	-23	-669
Mass (ton)		
Section	12.656	
Steel outfitting (7%)	0.886	
Safety coefficient (3%)	0.406	
Total weight	13.948	

The nonstructural mass property is used to represent a mass that won't affect the structural stiffness of the model. However, in this case, the difference between the actual mass and the mass measured by the FEMAP is considered as a nonstructural mass because adding the small outfitting details is not practical.

4.7 Meshing

The discretized model was created in the FEMAP on a non-geometry basis. Using the fabrication drawings as a guide, the creation of the discretized model was carried out. For members that have a specific shape such as holland profile, deck plating outline and all the curved shaped members, the outlines were exported as IGS. from the AutoCAD then imported to FEMAP and used as a guide to complete the mesh building. Different property colours are shown in Fig. 7.

Based on the frame spacing (500 mm) and guidance from industry experts (Mirel Balan, Structural Expert) it was recommended to use a global nesh density of 50 mm for most of the model. It is expected to find higher stress around the lifting lugs, a fine mesh density of 7 mm was applied on the lifting lugs to investigate the stress level. The global and local mesh samples are shown in Fig. 8. To make the stress field around the lifting lug hole more realistic, only the upper nodes of the hole were connected to the lifting sling, as presented in Fig. 9.
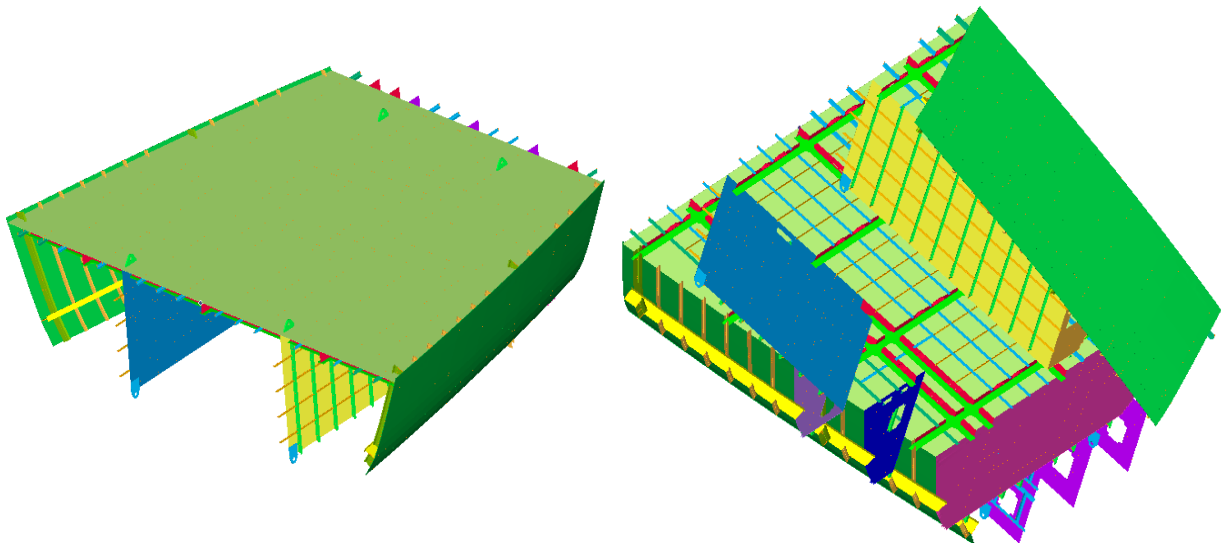
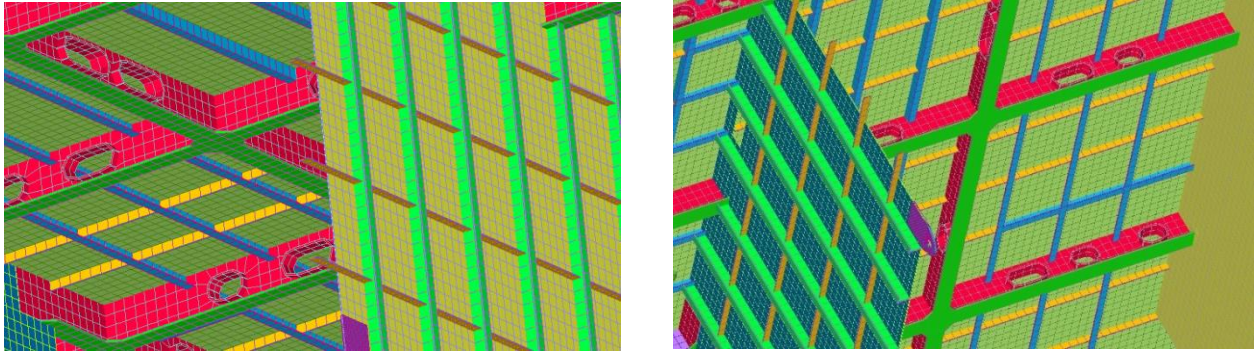Figure 7 Different structural property colours
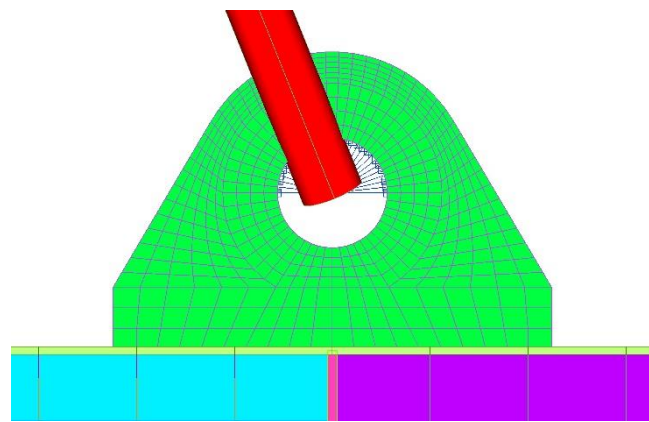
Figure 8 Global mesh

Figure 9 Mesh of the lifting lug

4.8 Element Types

The mesh has been built using a four-node shell element for all plating, deck transverses and girders. Three-node shell elements were used when necessary. Nastran rigid body elements (RBE2) were used to connect the lifting lug to the sling which is represented by a rod element. A bar element has been used to represent the secondary stiffeners attached to the deck, side and bulkheads. The holland profiles have been converted to the equivalent L-angle stiffeners and modelled as a bar element according to BV Rules for Steel Ships Pt B, Ch 4, Sec 3 (BV, 2020).The bar element has been widely used to reduce the computation requirements. However, the bar element carries only axial load which could be considered as an extra factor of safety.

4.9   Connections

Lifting lugs were connected to the ship section using "Glue connection" in FEMAP. Connection regions have been defined between the deck plating and the lifting lug and between the longitudinal bulkhead plating and the lifting lug. The glue connection is an effective method to represent the welding of two different mesh size regions. It accurately transfers displacement and loads at the interface. Thus, the strain and stress results are reliable. Grid points on glued edges and surfaces do not have to be coincident (PLM Software, n.d.). Fig. 10 shows the glue connection representing the fillet weld.
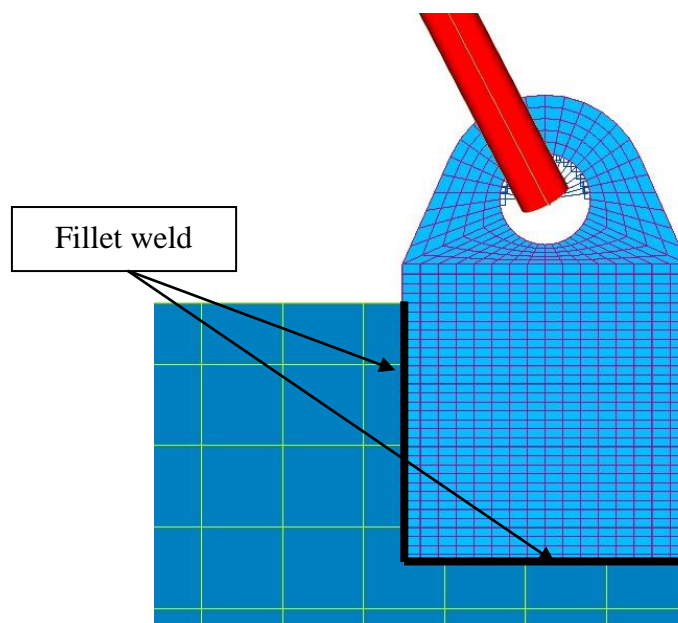
Fillet weld

Figure 10 Glue connection representing the fillet weld

4.10 Mesh Convergence

Convergence check of the stress results can be done at the high-stress location in the structure. If the difference between the elemental and nodal stress results is very small, one can say that the mesh is fine enough and the solution is convergent. It has been observed that the difference between the elemental and nodal stress at the highest stress location is around 3 MPa. Thus, this difference was considered negligible and the mesh is fine enough.

4.11 Constraints

Three sets of constraints have been applied in the adopted analysis. The first and second sets are similar and correspond to the simulations before and after turning. The suspension point that represents the crane hook was completely fixed. In addition, the centre nodes of the lifting lugs were constrained in X and Y directions. The first and second sets are displayed in Fig. 11, the shown numbers indicate the constrained degrees of freedom. The third set of constraints is for the worst-case scenario during turning. The suspension points and the centre nodes of the lifting lugs were constrained in all 6 degrees of freedom as shown in Fig. 12. It should be noted that the slings presence has no significant influence on the results in the turning load case.
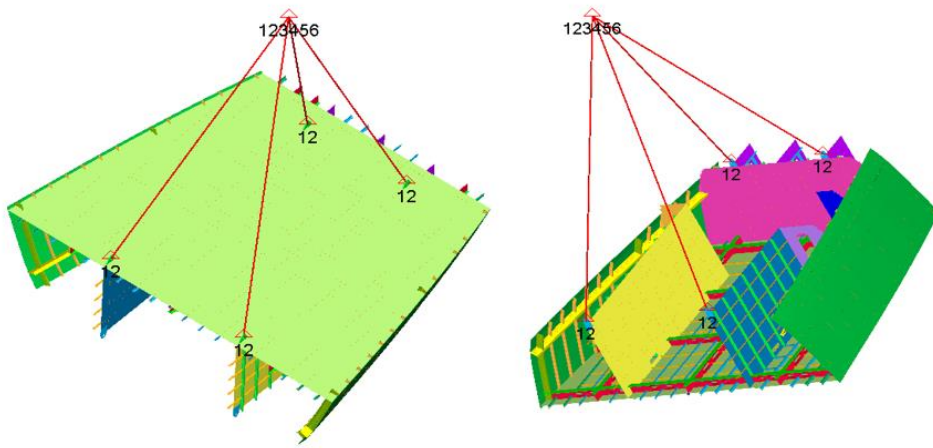

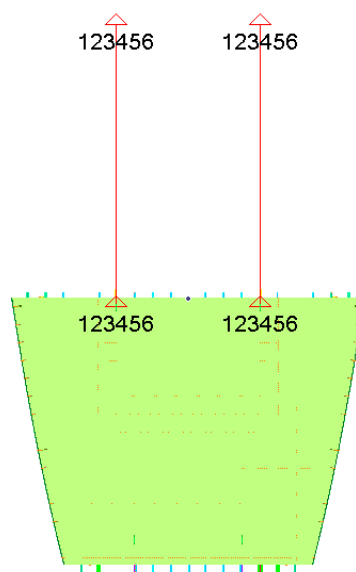Figure 11 Constraints for simulations before and after turning

Figure 12 Constraints for the turning case

4.12 Loading Conditions

4.12.1 Lifting Load

The analysis has been carried out under the gravity load for all three loading cases. The applied gravitational acceleration is acting downwards in the three cases. A dynamic amplification factor (DAF) of 1.5 has been applied according to DNVGL-RU-SHIP rules, resulting in an input magnitude of 14700 mm/s^2. For the turning load case, a new coordinate system was defined to simulate the equilibrium of the turning case. The X - axis passes through the centre of gravity and the centre nodes of the RBE2, the load was applied in the X - direction. The original and new coordinate systems are shown in Fig. 13.
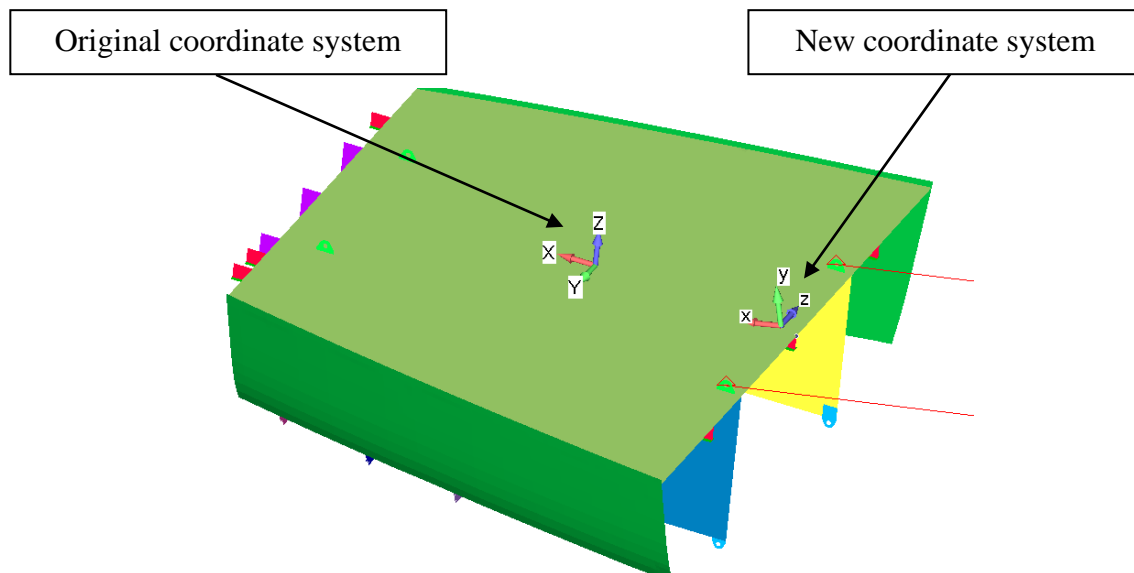
Figure 13 Original and new coordinate systems

4.12.2 Load Cases

The model was solved for a total of six load cases. Peak Von-Mises stress and deformations were extracted from the analysis outcomes for each load case. The section was firstly analyzed without the temporary stiffening (three load cases) which was then added to the model for further second analysis (three load cases). The analysed load cases are summarized in Table 3.

Table 3 Load cases

Load Case	Description
Without temporary stiffening	
Load Case 1 (LC1)	Lifting before turning
Load Case 2 (LC2)	Turning load case
Load Case 3 (LC3)	Lifting after turning
With temporary stiffening	
Load Case 4 (LC4)	Lifting before turning
Load Case 5 (LC5)	Turning load case
Load Case 6 (LC6)	Lifting after turning

4.13 Acceptance Criteria

The analysis has been carried out following the guidelines from DNVGL-CG-0127 and the DNVGL rules for the Classification of Ships Part 3. Chapter 7. The stress acceptance criteria for the lifting cases are to comply with the DNVGL mentioned rules and are summarized in Table 4. The obtained plate elemental Von Mises stress is to be compared with the acceptance criteria. For the bar elements, the comparison should be based on the combined stress (DNV GL, 2015).

Table 4 Acceptance criteria summary (DNV GL, 2018)

Case	Description	Element		Acceptance criteria	
				% Of yield stress	Allowable stress (MPa)
AC-1	Static	Coarse mesh plate/beam element		80	188
		Fine shell element mesh (Average over 50 mm x 50 mm area)	Vicinity of welding seems	120	282
			Far from welding	163	320

The obtained stress results from the FE analysis are to be compared with the acceptance criteria in the fine mesh zones as follows:

$$\gamma_f \leq \gamma_{fperm}$$

$$\gamma_f = \frac{\sigma_{vm}}{R_Y} \; for \; plate \; elements \; in \; general.$$

$$\gamma_f = \frac{\sigma_{axial}}{R_Y} \; for \; rod \; elements \; in \; general.$$

Where,

$\gamma_f = Fine \; mesh \; yield \; utilization \; factor.$
$\sigma_{vm} = Von \; Mises \; sress, in \; N/mm^2.$
$\sigma_{axial} = Axial \; sress \; in \; rod \; element, in \; N/mm^2 .$
$\sigma_{fperm} = Permissible \; fine \; mesh \; utilization \; factor = 1.$
$R_Y = Nominal \; yield \; stress, taken \; equal \; to \; 235/k \; N/mm^2.$

The above yield allowance accounts for the simplification in the elastic theory used by the linear FEA where the material is assumed to be perfectly elastic. the far beyond yield stress predicted by the linear FEA, in reality, redistribute through yielding (plastic deformation) in the nearby elements resulting in less stress yet higher strain. this has to do with the actual nonlinear ductile behaviour of steel where the material follows a progressive stress-strain relationship. Hence, class rules allow margins within which elements beyond yield stresses from the linear FEA are accepted.

5 RESULTS AND DISCUSSION

5.1 Lifting the Section Before Turning (LC1)

At the ship construction site, the sections are built upside down to avoid the overhead welding as possible to fasten the fabrication process and reduce the cost of production. The section is to be lifted using one crane, with four slings of eight meters long each.

The stresses throughout the analyzed model remain below the fine mesh allowable stress of 282 MPa (AC-I adjacent to weld), indeed the majority remain under 24 MPa, increasing to a peak value of 107.49 MPa in way of the lifting lugs. The contour plot of the maximum Von Mises stress for the plate top and bottom of load case LC1 are shown in Fig. 14. It should be noticed that the solving time is very short due to the act of using the bar element to represent all the stiffeners

The section experienced a total maximum deflection of 16.44 mm in way of the aft boundary of the section as shown in Fig. 15. It is observed that supporting stiffeners are needed to be fitted at the position of the maximum translation. The maximum translation in the X, Y, and Z directions are –7 mm, -9.5 mm and 16.1 mm respectively.

Output Set: BEFORE TURNING W/O TEMPORARY STIFFENING
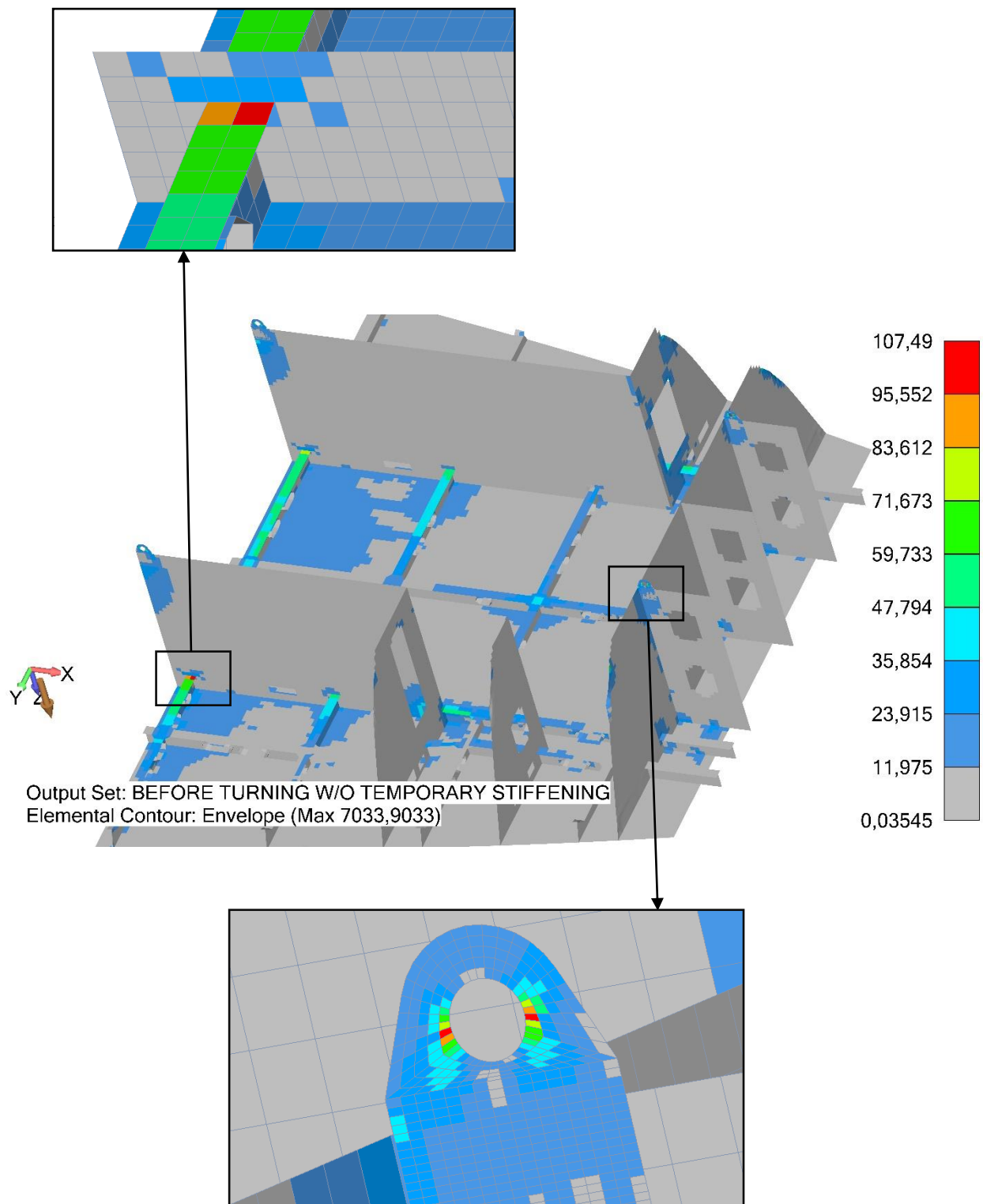Elemental Contour: Envelope (Max 7033,9033)

Figure 14 Maximum of Plate top/Plate bottom Von Mises stress – lifting before turning without temporary stiffening
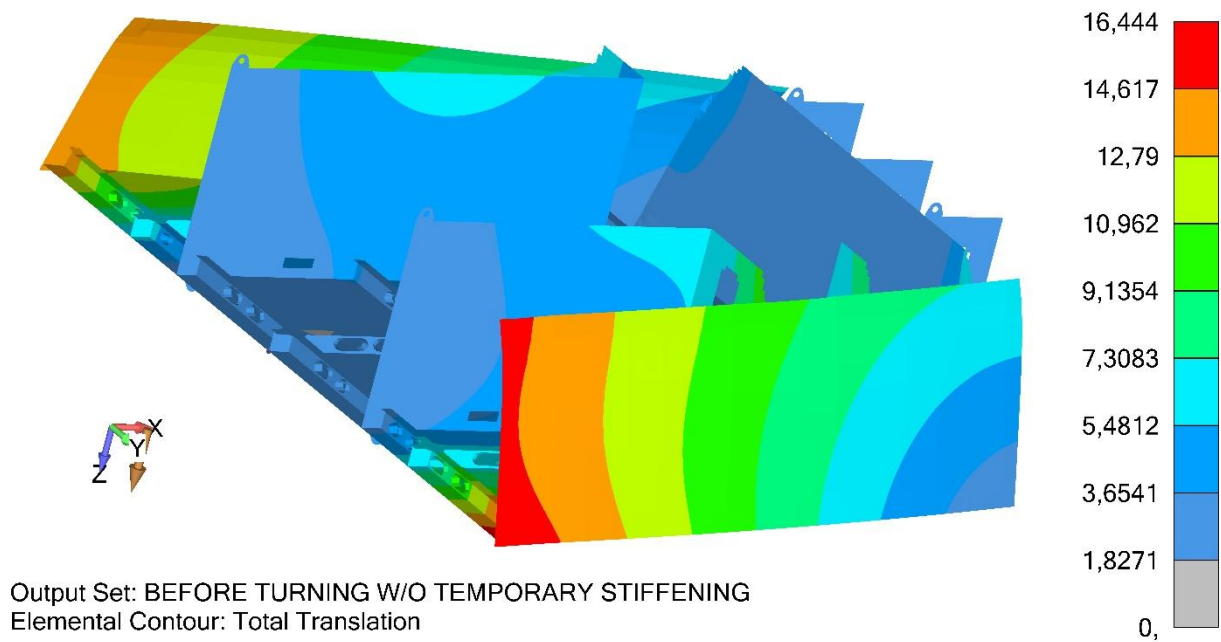
Figure 15 Total translation – lifting before turning without temporary stiffening

5.2 Turning the Section (LC2)

The section is suspended from only two lifting lugs as shown in Fig. 16 and using only two slings, which is the worst-case during the turning process. The stresses remain below the fine mesh allowable stress of 282 MPa (AC-I adjacent to weld), the majority remain under 23 MPa, increasing to a peak value of 209.1 MPa in way of the two lifting lugs. The contour plot of the maximum Von Mises stress for the plate top and bottom of load case LC2 are shown in Fig. 16.

The section experienced a total maximum deflection of 6.8 mm as shown in Fig. 17. It is observed that supporting stiffeners are needed to be fitted longitudinally at the position of the maximum translation. The maximum translation in the X, Y, and Z directions are 5.9, -4.4 mm and -5.88 mm respectively.
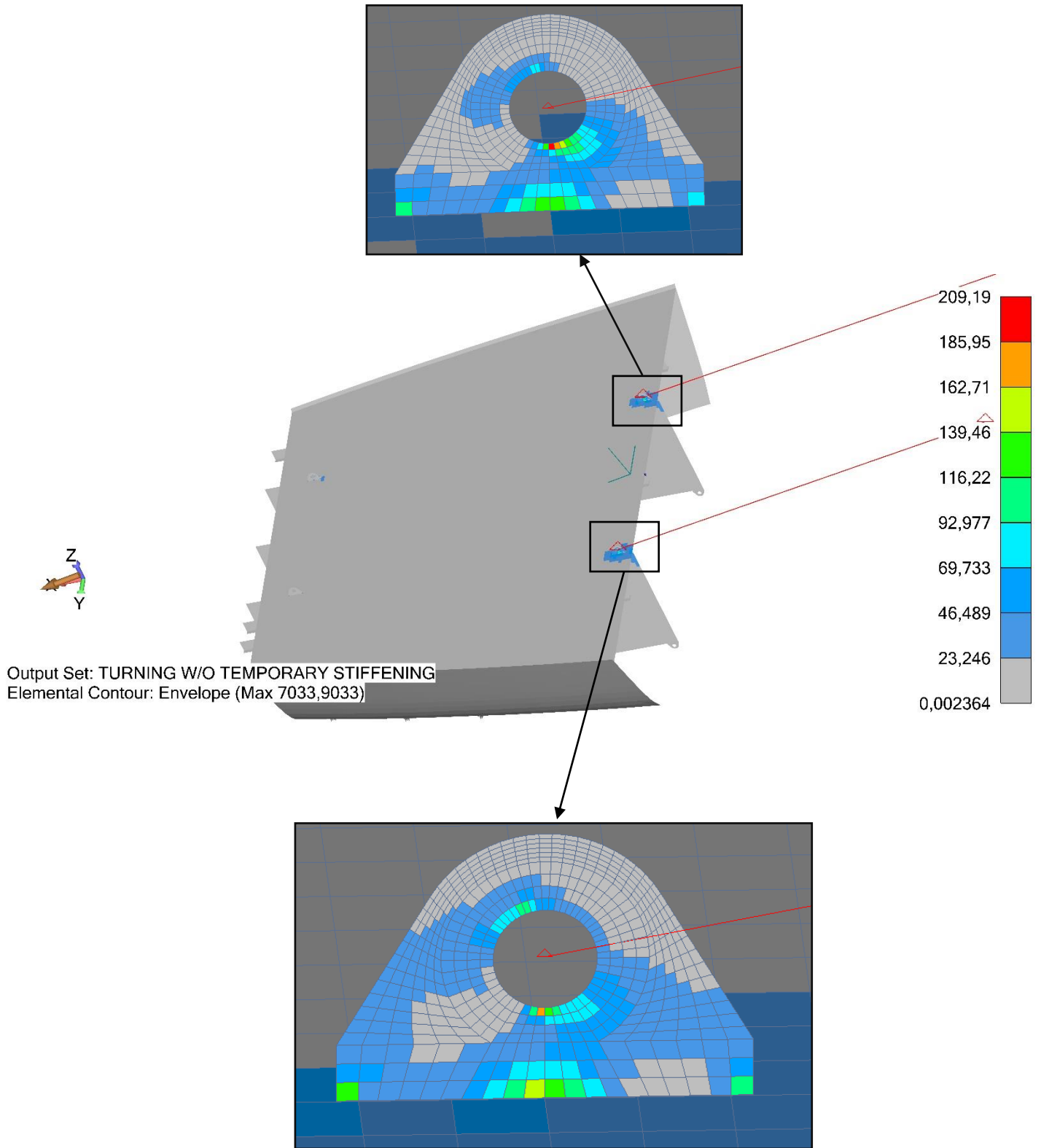
Figure 16 Maximum of Plate top/Plate bottom Von Mises stress –turning case without temporary stiffening
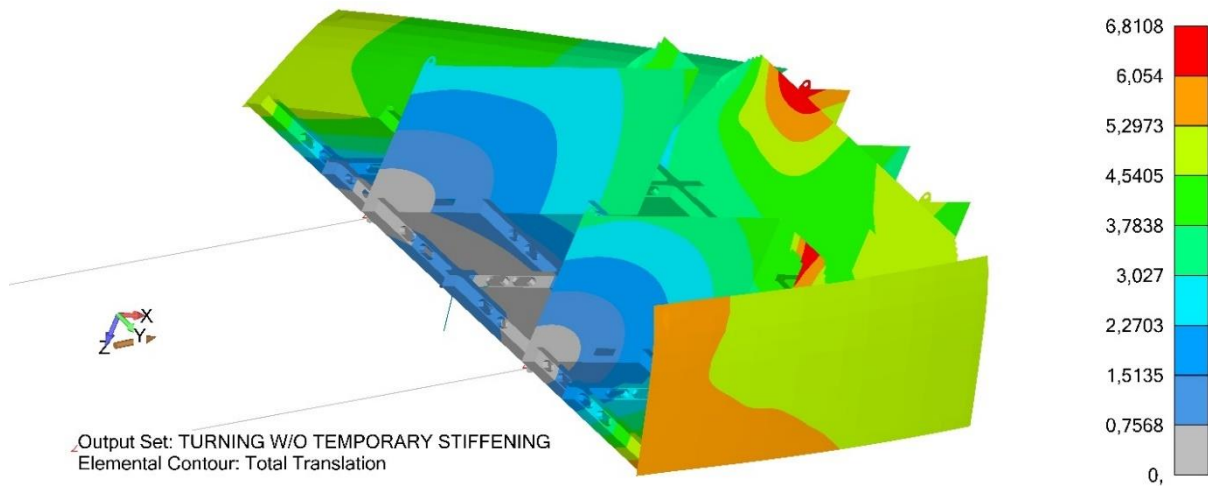
Figure 17 Total translation – turning without temporary stiffening

5.3 Lifting the Section After Turning (LC3)

The stresses remain below the fine mesh allowable stress of 282 MPa (AC-I adjacent to weld), indeed the majority remain under 26 MPa, increasing to a peak value of 275.7 MPa in way of the lifting lugs. The contour plot of the maximum Von Mises stress for the plate top and bottom of load case LC3 are shown in Fig. 18.

The total maximum deflection is 16.44 mm in way of the aft boundary of the section as shown in Fig. 19. It is observed that supporting stiffeners are needed to be fitted transversely and vertically at the position of the maximum deformation. The maximum translation in the X , Y, and Z directions are 4.5 mm, 9.7 mm and 15.2 mm respectively.
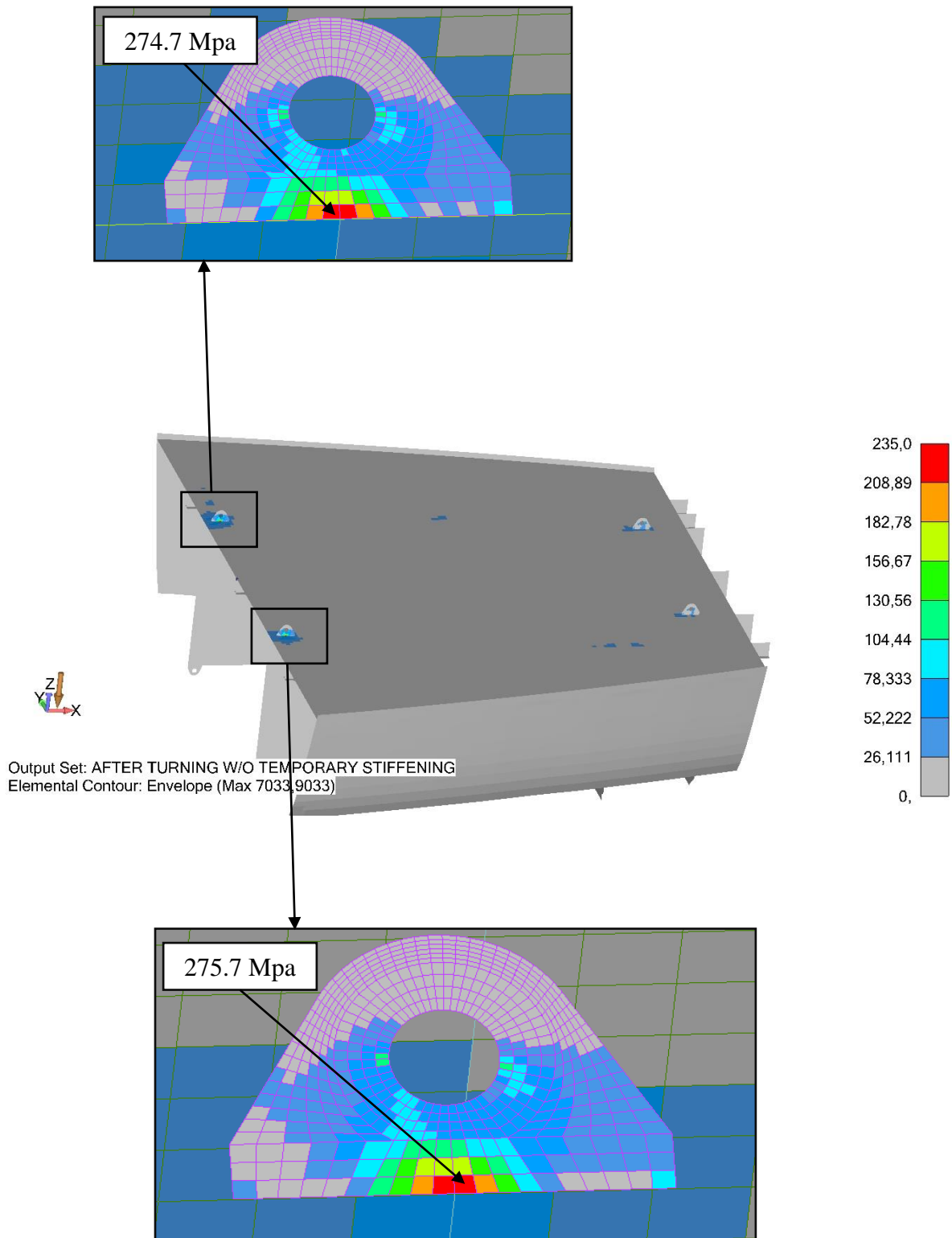
274.7 Mpa

275.7 Mpa

Output Set: AFTER TURNING W/O TEMPORARY STIFFENING
Elemental Contour: Envelope (Max 7033,9033)

Figure 18 Maximum of Plate top/Plate bottom Von Mises stress – lifting after turning without temporary stiffening

Output Set: AFTER TURNING W/O TEMPORARY STIFFENING
Elemental Contour: Total Translation
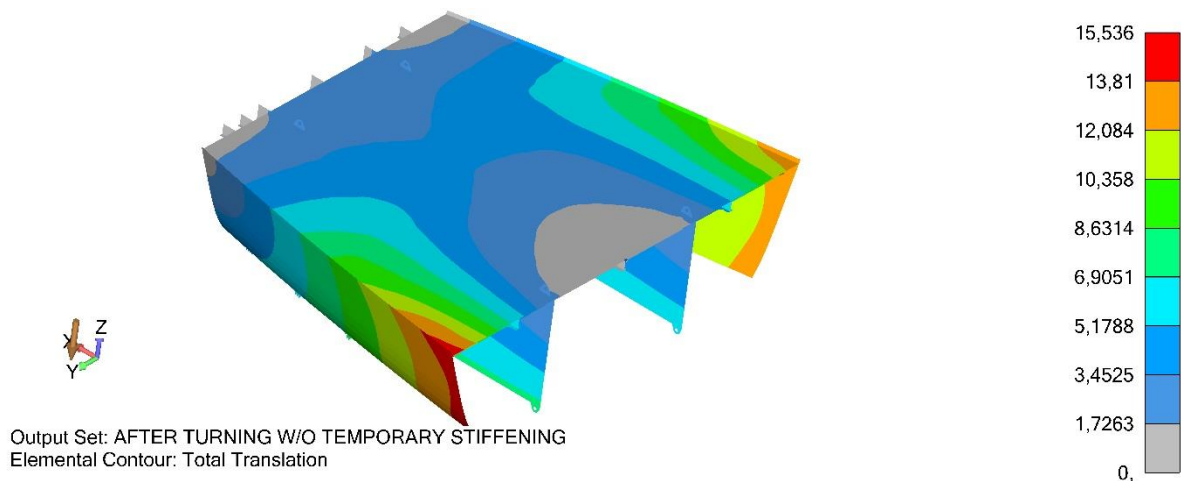
Figure 19 Total translation – lifting after turning without temporary stiffening

5.4   Lifting the Section Before Turning (LC4)

After adding the temporary stiffening according to the lifting plan, the stresses are also remaining below the fine mesh allowable stress of 282 MPa (AC-I adjacent to weld), increasing to a peak value of 105.9 MPa in way of the lifting lugs. The contour plot of the maximum Von Mises stress for the plate top and bottom of load case LC4 are shown in Fig. 20. It should be noted that the stress has slightly decreased compared to the same lifting process without temporary stiffening.

In this case, the obtained total maximum deflection is 8.2 mm in way of the aft boundary of the section and at the position of the temporary stiffeners as shown in Fig. 21. It is observed that the temporary stiffeners have significantly affected the deformation characteristics of the section. The maximum translation in the X, Y, and Z directions are 4.5 mm, 9.7 mm and 15.2 mm respectively.
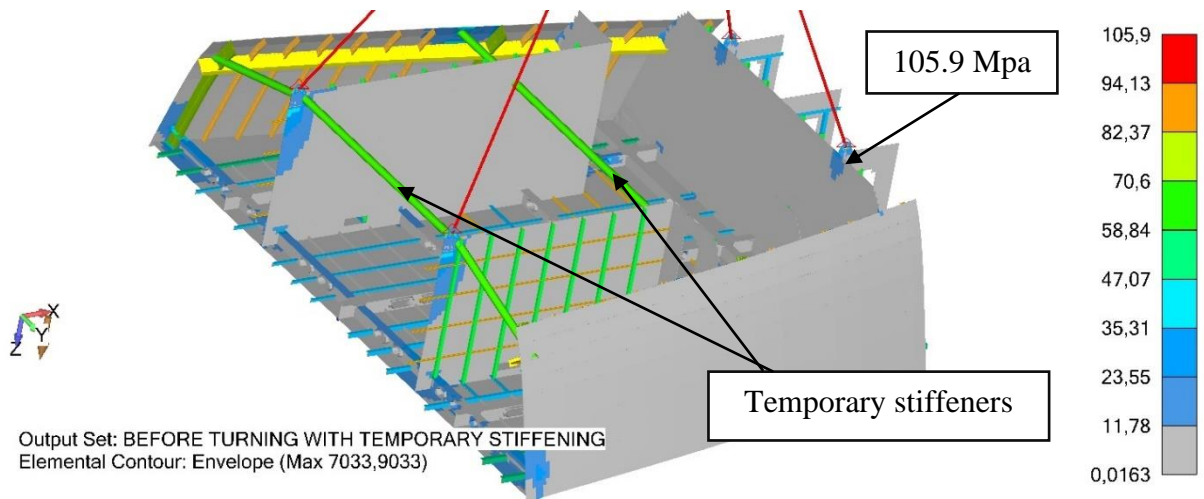
105.9 Mpa

Temporary stiffeners

Output Set: BEFORE TURNING WITH TEMPORARY STIFFENING
Elemental Contour: Envelope (Max 7033,9033)

Figure 20 Maximum of Plate top/Plate bottom Von Mises stress – lifting before turning with temporary stiffening

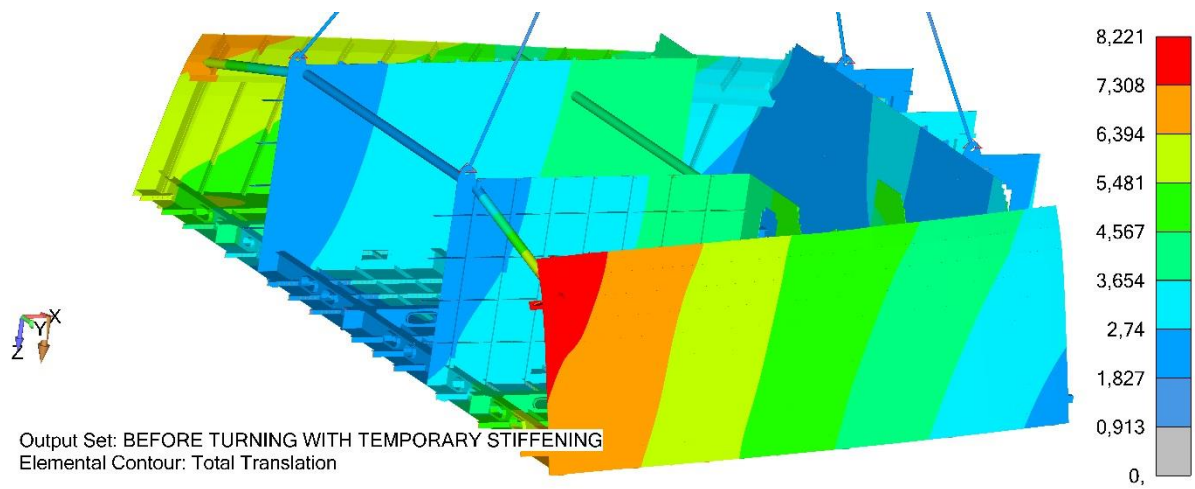Output Set: BEFORE TURNING WITH TEMPORARY STIFFENING
Elemental Contour: Total Translation

Figure 21 Total translation – lifting before turning with temporary stiffening

5.5 Turning the Section (LC5)

In the worst-case during turning after adding the temporary stiffening according to the lifting plan, the stresses remained below the fine mesh allowable stress of 282 MPa (AC-I adjacent to weld), increasing to a peak value of 183.79 MPa in way of the two lifting lugs. The contour plot of the maximum Von Mises stress for the plate top and bottom of load case LC5 are shown in Fig. 22.

In this case, the obtained total maximum deflection is 6.69 mm as shown in Fig. 23. It is observed that the temporary stiffeners have no influence on the deformation characteristics of the section. The maximum translation in the X , Y, and Z directions are 3.66 mm, -1.1 mm and -6.8 mm respectively.
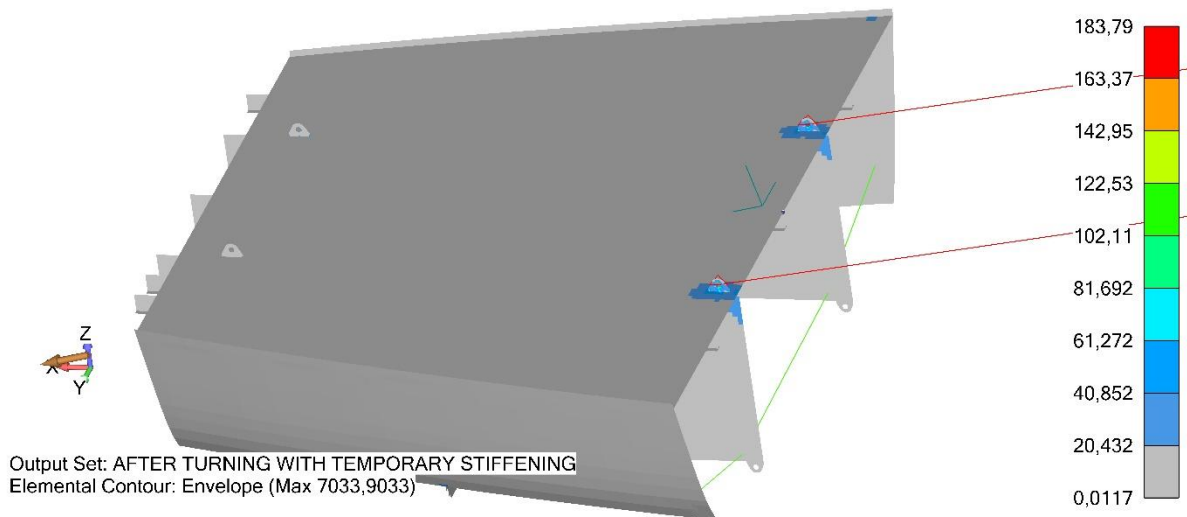

Output Set: AFTER TURNING WITH TEMPORARY STIFFENING
Elemental Contour: Envelope (Max 7033,9033)

Figure 22 Maximum of Plate top/Plate bottom Von Mises stress –turning case with temporary stiffening

Output Set: AFTER TURNING WITH TEMPORARY STIFFENING
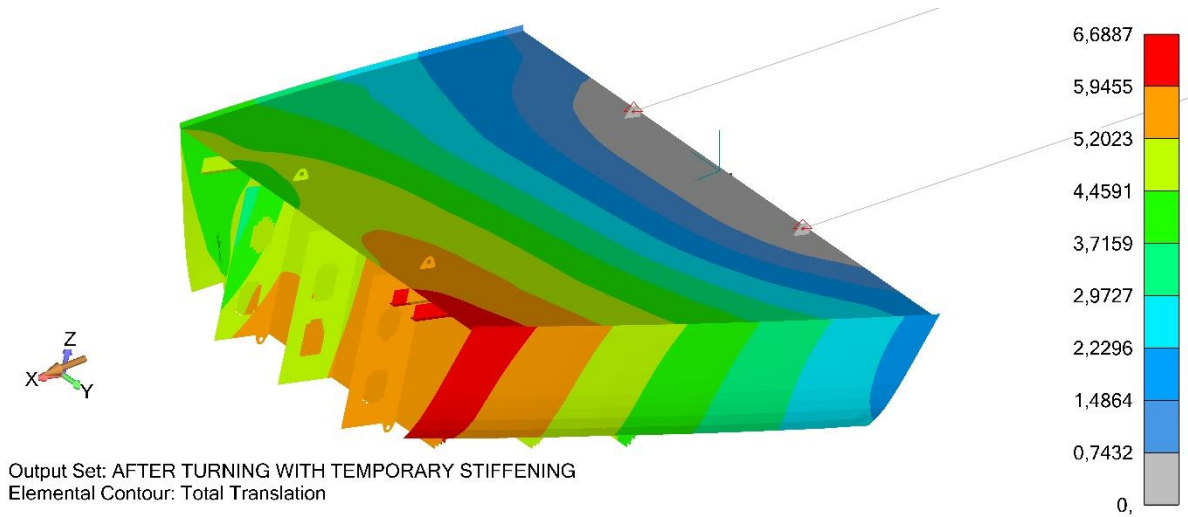Elemental Contour: Total Translation

Figure 23 Total translation – turning with temporary stiffening

5.6 Lifting the Section After Turning (LC6)

For the case of lifting after turning with the temporary stiffening, the stresses remained below the fine mesh allowable stress of 282 MPa (AC-I adjacent to weld), increasing to a peak value of 123.79 MPa in way of the lifting lugs. The contour plot of the maximum Von Mises stress for the plate top and bottom of load case LC6 are shown in Fig. 24.

Output Set: AFTER TURNING WITH TEMPORARY STIFFENING
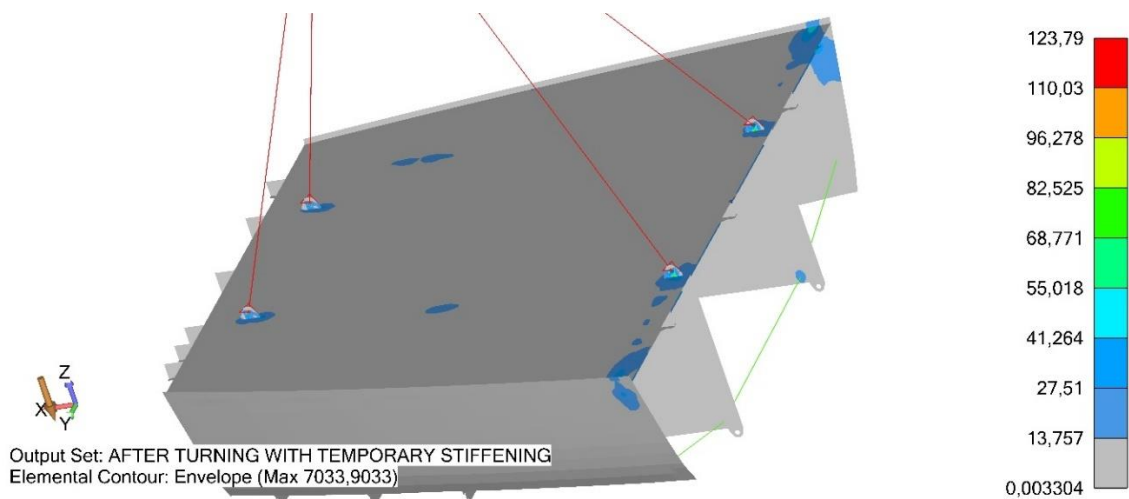Elemental Contour: Envelope (Max 7033,9033)

Figure 24 Maximum of Plate top/Plate bottom Von Mises stress – lifting after turning with temporary stiffening

In this case, the obtained total maximum deflection is 7.41 mm as shown in Fig. 25. It is observed that the temporary stiffeners have a significant influence on the deformation characteristics of the section. The maximum translation in the X, Y, and Z directions are 1.7 mm, -2.5 mm and -7.2 mm respectively.
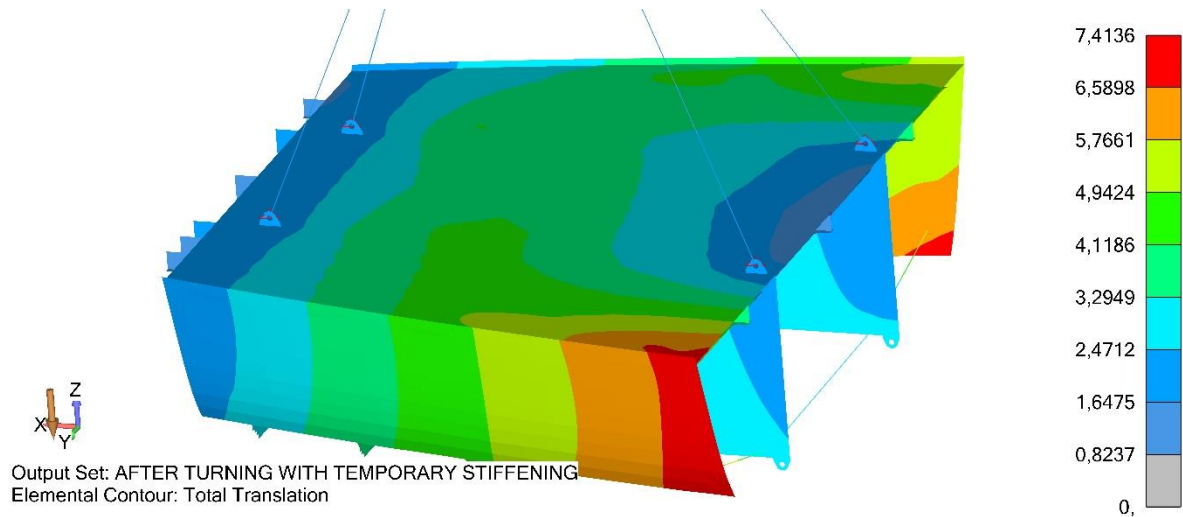

Figure 25 Total translation – lifting after turning with temporary stiffening

5.7   Comparison of Load Cases

Fig. 26 compares the maximum Von Mises stress values of all the six load cases. It is observed that the temporary stiffening has a negligible effect on reducing stresses while lifting the section before turning. In the worst-case during turning the temporary stiffening slightly improved the stress field by reducing the peak stress by 12.1 % (25.4 MPa). However, for lifting after turning, the temporary stiffening has a significant influence on mitigating the maximum stresses by 55 % (151.9 MPa). Accordingly, stress-wise, this demonstrates the importance of adding the temporary stiffening in the final stage of lifting.
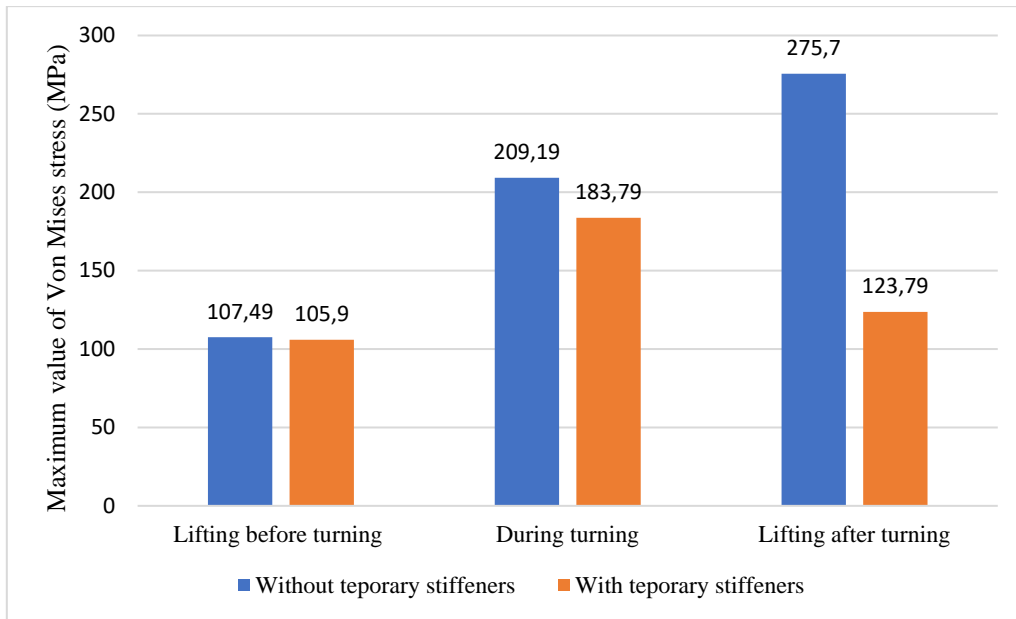
Figure 26 Comparison of maximum Von Mises stress

Regarding the total deflection, not only the temporary stiffening significantly improved the lifting after turning operation but also improved the lifting before tuning operation. However, the turning operation has not been affected by the existence of the temporary stiffening. This is justified because the temporary stiffeners are needed for resisting deformations in the longitudinal direction as indicated Fig. 17. which has a minimum effect on the turning load path. Fig. 27 shows a comparison of maximum deformation for all the six loading cases.
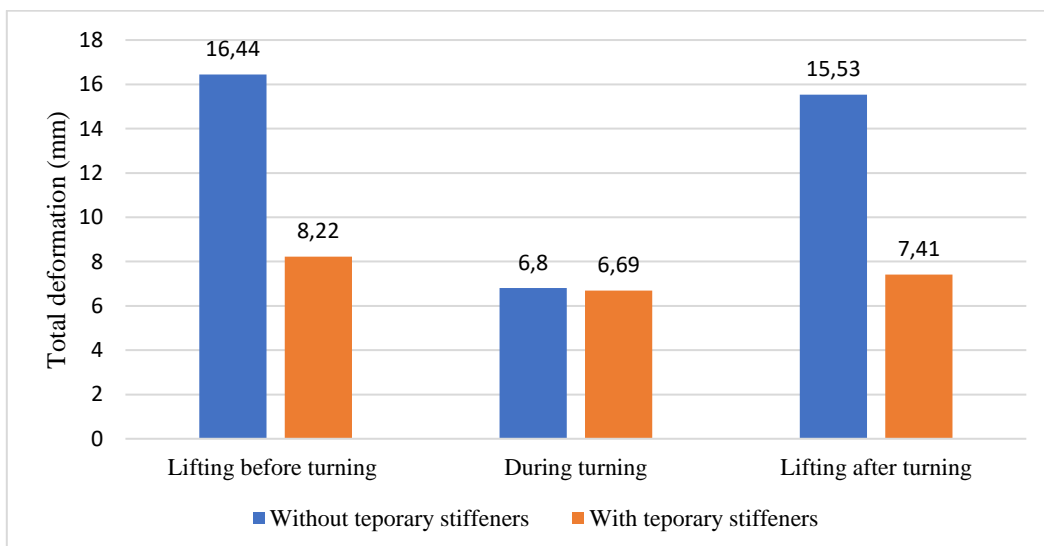

Figure 27 Comparison of maximum deformation

5.8 Sling Angle analysis

The hook position should be placed above the center of gravity. Otherwise, the section will tilt until the hook and the center of gravity become on the same vertical line. The uneven stable position could lead to different sling angles and therefore different structural behaviour. Tilting the section might break the sling and/ or the weld of the lug. Also, it might cause more deformations on the section(Petri Mehto, 2019)

The sling angle is the angle between the sling and the horizontal line of the ship section deck. Different sling angles have been studied to investigate the sling angle effect on the stress levels and deformations during the lifting of the ship section with the temporary stiffening. It has been observed that the stress is inversely proportional to the increase of the sling angle. However, the stress reduction is from 83.9 MPa at 30 degrees to 83.35 MPa at 75 degrees. Therefore, the stress variation is negligible. Fig. 28 shows the sling angle – maximum Von Mises stress relationship.
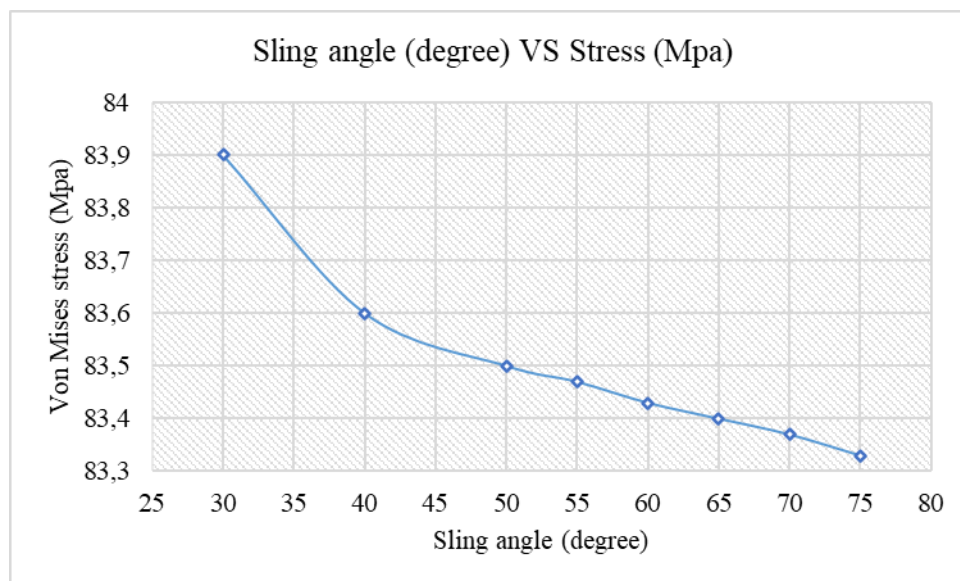

Figure 28 Sling angle - Maximum Von Mises stress

Sling length is mainly dependent on the optimized sling angle which maintains the stress below the yield limit to remain in the elastic deformation zone of the structure. Also, the crane specification is important for the determination of the distance between two adjacent lifting lugs was adjusted. For a given position of the lifting lugs, the length of the fore and aft lifting slings is calculated to ensure that there is no trim angle during the lifting process.

The best sling angle would lay between 55 and 65 degrees as shown from the results in Fig. 29, to compromise the sling tension force after resolving it, the horizontal component of the sling force decreases as the sling angle increases. Thus, reduce the probability of buckling. However, the vertical component of the sling force increases as the sling angle increases. Thus, the structure will experience more bending load.
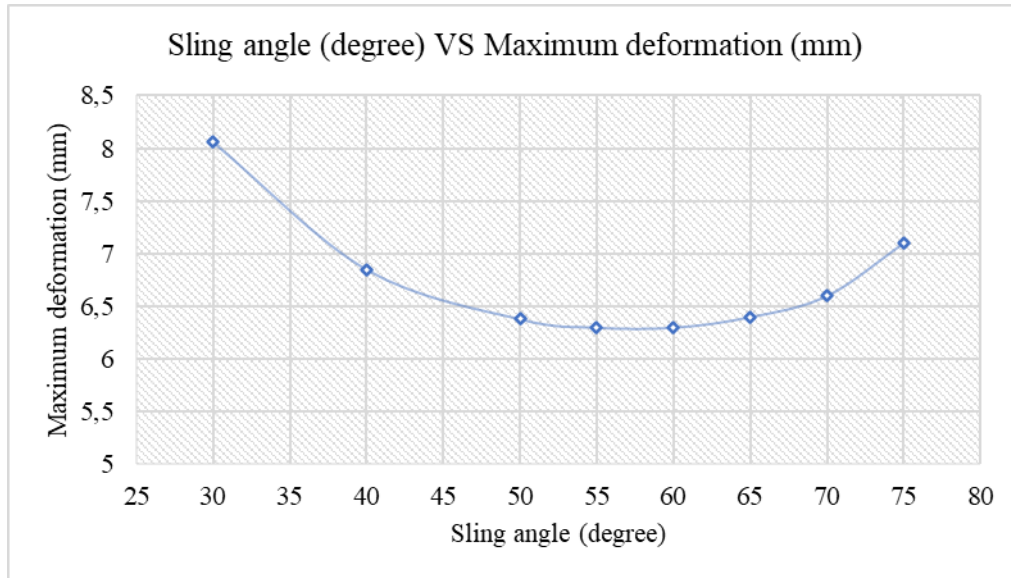

Figure 29 Sling angle - Maximum deformation

6   CONCLUSIONS

The lifting and turning of section 1172 have been simulated in FEMAP software. A linear static analysis was carried out using Simcenter^{TM} Nastran solver to investigate the deformations and stresses for six different loading cases. First, the section has been analysed without temporary stiffening in three load scenarios: lifting before turning, worst-case scenario during turning and lifting after turning. Similarly, the section has been analysed after adding the temporary stiffening according to the lifting plan. The following conclusions are withdrawn:

- As expected, the stress hotspots are located in way of the lifting lugs. The majority of the stresses remained under the yield stress of 235 MPa. Also, the addition of temporary stiffening is essential to minimize the deformations and to maintain the stress levels below the yield point.

- The lifting plan design requires a high technical level of engineers. The designer needs to comprehensively consider the characteristics of the selected section, the site conditions, crane lifting capacity, lifting lugs reusability and other constraints (each case might have special requirements) are required to complete the design of the lifting plan.

- When the hull sections are assembled, if the length of slings is properly selected, the free angle of the section after lifting can be exactly adjusted to meet the inclination of the hull by using the selected crane under the condition that the crane load is allowed. Thus, it is advantageous to reduce the labour intensity and reduce the assembly time.

- In order to achieve high quality in the shortest time possible, the unusual shape sections should be analyzed one by one. Specialized FEM engineers are needed with knowledge and experience in lifting operations. In addition, a fast and reliable analysis can be carried out with proper software.

- The non-geometry base FE modelling is a special case, it should be used only when the 3D surface model does not exist. The geometry-based modelling has the advantages of modifying, refine the mesh faster and make use of many features of the FEA software. Moreover, working with a geometry-based problem is faster and easier.

7 BIBLIOGRAPHY

Alsayed, M., & Ismail, I. (2019). *From Linear to Nonlinear Finite Element Analyses for Enhancing Design Assessment of Ships' Structural Details with Cut-outs. Master thesis. University of Southampton*.

Azad, N., Iranmanesh, M., & Rahmati Darvazi, A. (2020). A study on the effect of welding sequence on welding distortion in ship deck structure. *Ships and Offshore Structures*, *15*(4), 355–367. https://doi.org/10.1080/17445302.2019.1619898

Batista, H. S. (2012). *Analysis and prediction of welding deformations of ship panels in prefabrication process. Master thesis. University of Technology, Szczecin*.

BV. (2020). *PART B-Hull and Stability Rules for the Classification of Steel Ships*. https://marine-offshore.bureauveritas.com/bv-rules

Chun, D.-H., Roh, M.-I., Ham, S.-H., & Lee, H.-W. (2018). A Study on the Methods for Finding Initial Equilibrium Position of a Lifting Block for the Safe Erection. *Journal of the Society of Naval Architects of Korea*, *55*(4), 297–305. https://doi.org/10.3744/snak.2018.55.4.297

Damen Shipyards Galati report. (n.d.). *Transport, handling and manoeuvring of various materials, pieces, structures, aggregates and equipment in storages, shops and at ships*.

DNV GL. (2015). *CLASS GUIDELINE Finite element analysis*. http://www.dnvgl.com,

DNV GL. (2018). *RULES FOR CLASSIFICATION Ships*. http://www.dnvgl.com,

Galatanu, L., Gavan, E., & Georgiana DARIE, A. (2020). *Stress and strain analysis that occurs in the structure of a section and in its lifting installation, during the lifting and turning maneuvers*.

Hammad, A., Abdel-Nasser, Y., & Shama, M. (2021). Rational Design of T-Girders via Finite Element Method. *Journal of Marine Science and Application*, *20*(2), 302–316. https://doi.org/10.1007/s11804-021-00206-1

Hammad, A., Churiaque, C., Sánchez-Amaya, J. M., & Abdel-Nasser, Y. (2021). Experimental and numerical investigation of hybrid laser arc welding process and the influence of welding sequence on the manufacture of stiffened flat panels. *Journal of Manufacturing Processes*, *61*, 527–538. https://doi.org/10.1016/j.jmapro.2020.11.040

https://www.makeitfrom.com/material-properties/EN-1.0308-E235-Non-Alloy-Steel. (2020).

Jang, C. D., Lee, C. H., & Ko, D. E. (2002). *Prediction of welding deformations of stiOEened panels*.

Lee, H., Roh, M. il, & Ham, S. H. (2016). Block turnover simulation considering the interferences between the block and wire ropes in shipbuilding. *Automation in Construction*, *67*, 60–75. https://doi.org/10.1016/j.autcon.2016.03.013

Li Rui, Zhang Fan, Liu Yujun, & Jiang Fumao. (2013). *Design system for ship block lifting with Computer-aided. China Academic Journals Electronic Publishing House. 9. 3.*

Mandal, N. R. (2017). *Ship Construction and Welding. Springer Series on Naval Architecture, Marine Engineering, Shipbuilding and Shipping 2.*

Petri Mehto. (2019). *Optimized analysis method for hoisting design of large steel structures. Bachelor´s thesis.Turku university of applied sciences.*

PLM Software, S. (n.d.). *Femap Assembly Modeling white paper*. www.siemens.com/plm

Ponthot, J. P. (2020). *AN INTRODUCTION TO THE FINITE ELEMENT METHOD 1.*

Samin. CO. (2013). *Dimensional control for shipbuilding and marine(Online). Availble from: https://www.youtube.com/watch?v=Tk27BSv7B-k.*

Wang, J., Rashed, S., Murakawa, H., & Luo, Y. (2013). Numerical prediction and mitigation of out-of-plane welding distortion in ship panel structure by elastic FE analysis. *Marine Structures*, *34*, 135–155. https://doi.org/10.1016/j.marstruc.2013.09.003

Wang, J., Yi, B., & Zhou, H. (2018). Framework of computational approach based on inherent deformation for welding buckling investigation during fabrication of lightweight ship panel. *Ocean Engineering*, *157*, 202–210. https://doi.org/10.1016/j.oceaneng.2018.03.057

Wang, J., Yuan, H., Ma, N., & Murakawa, H. (2016). Recent research on welding distortion prediction in thin plate fabrication by means of elastic FE computation. *Marine Structures*, *47*, 42–59. https://doi.org/10.1016/j.marstruc.2016.02.004

Yi, M. S., Lee, D. H., Lee, H. H., & Paik, J. K. (2020). Direct measurements and numerical predictions of welding-induced initial deformations in a full-scale steel stiffened plate structure. *Thin-Walled Structures*, *153*. https://doi.org/10.1016/j.tws.2020.106786

APPENDICES
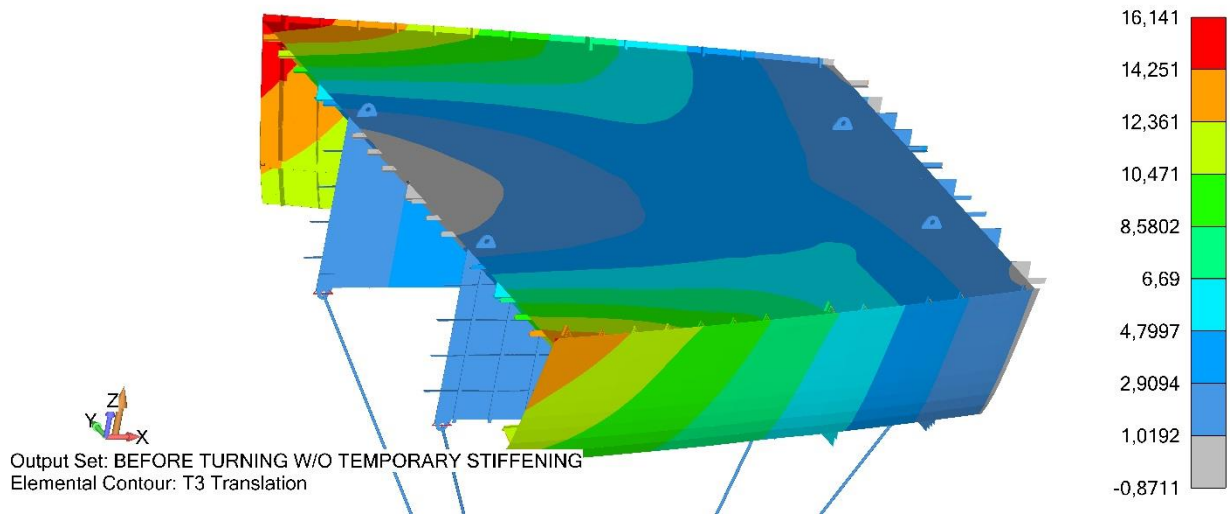
Appendix 1. X - direction translation – lifting before turning without temporary stiffening
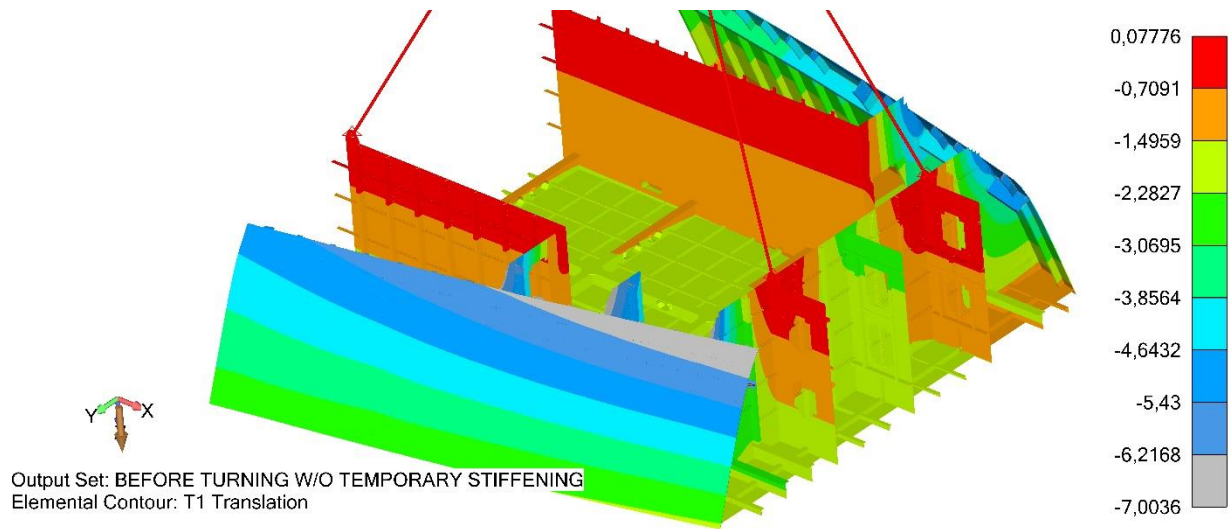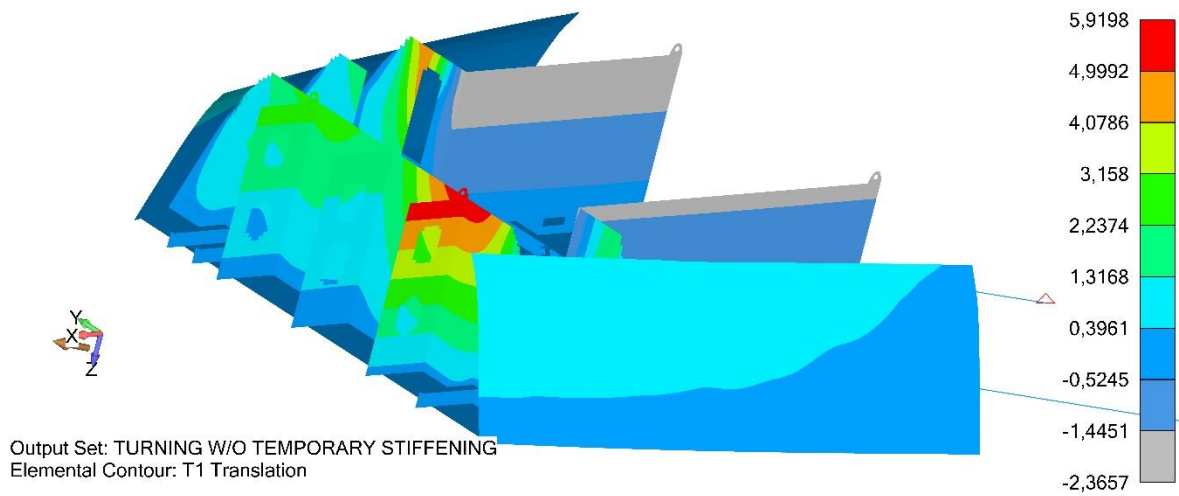

Appendix 2. Y- direction translation – lifting before turning without temporary stiffening
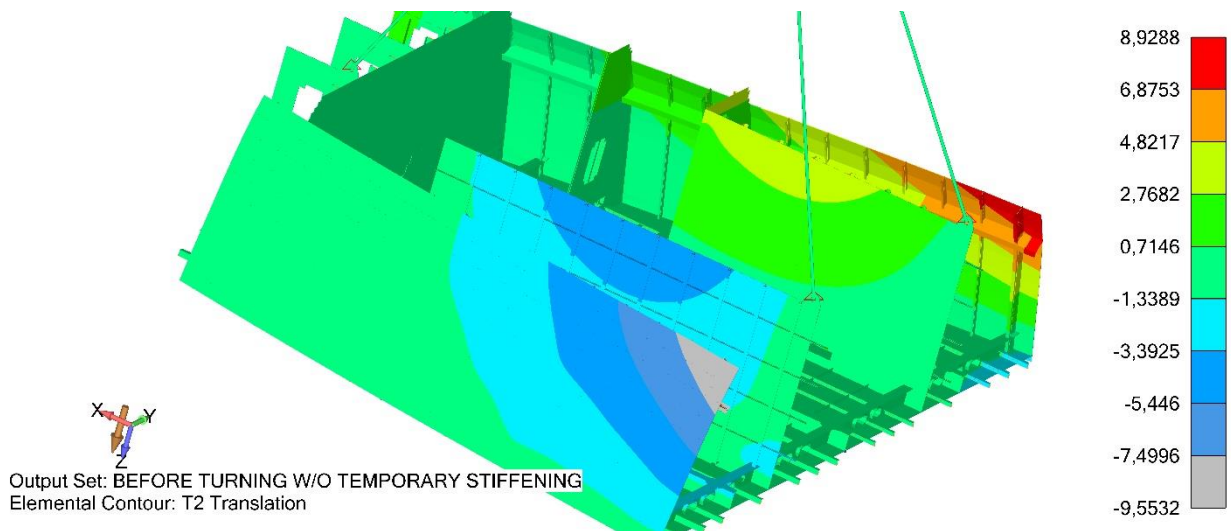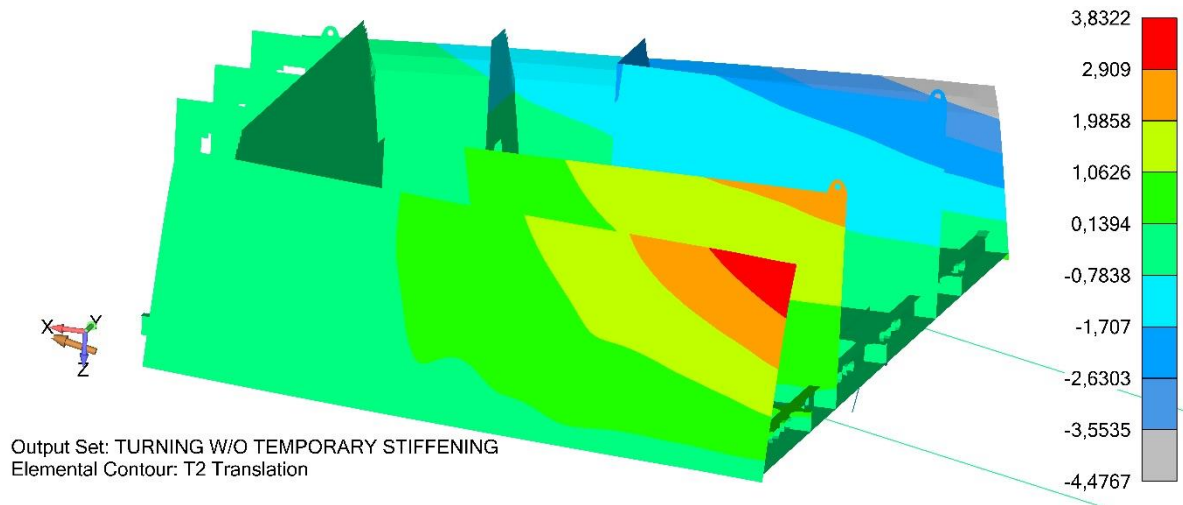
Appendix 3. Z - direction translation – lifting before turning without temporary stiffening
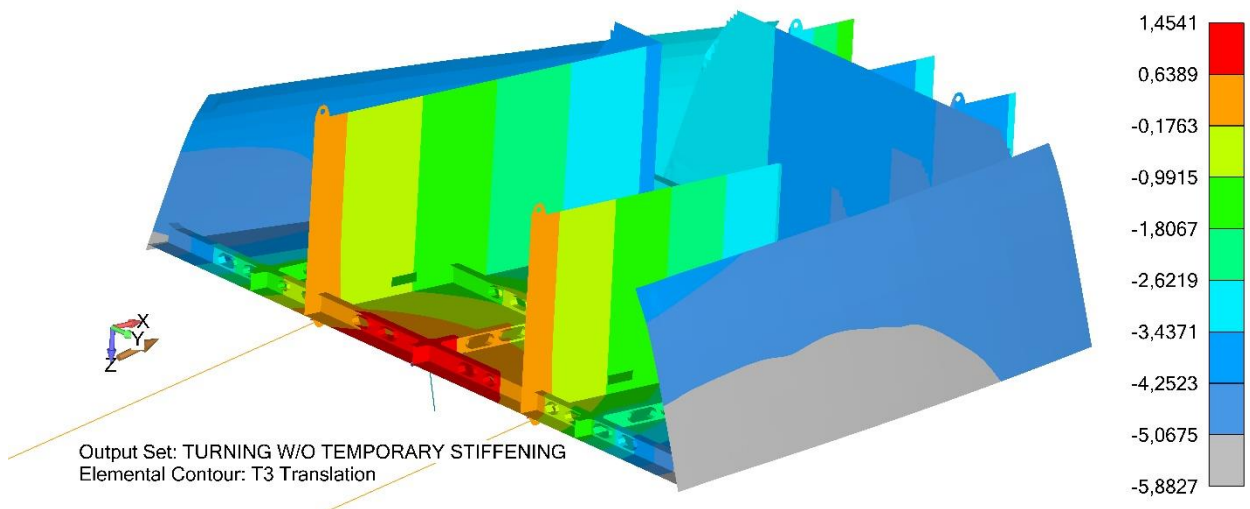

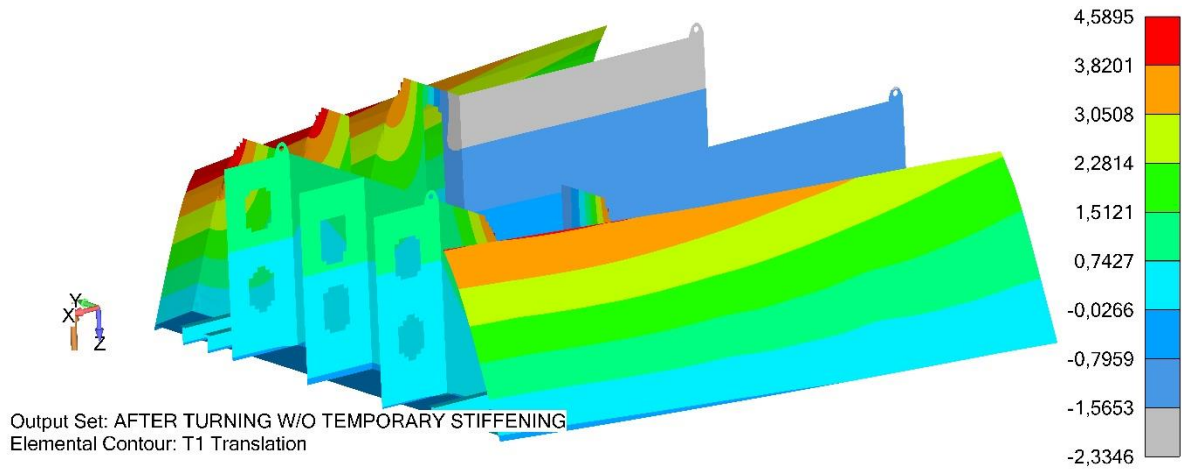Appendix 4. X direction translation – turning without temporary stiffening

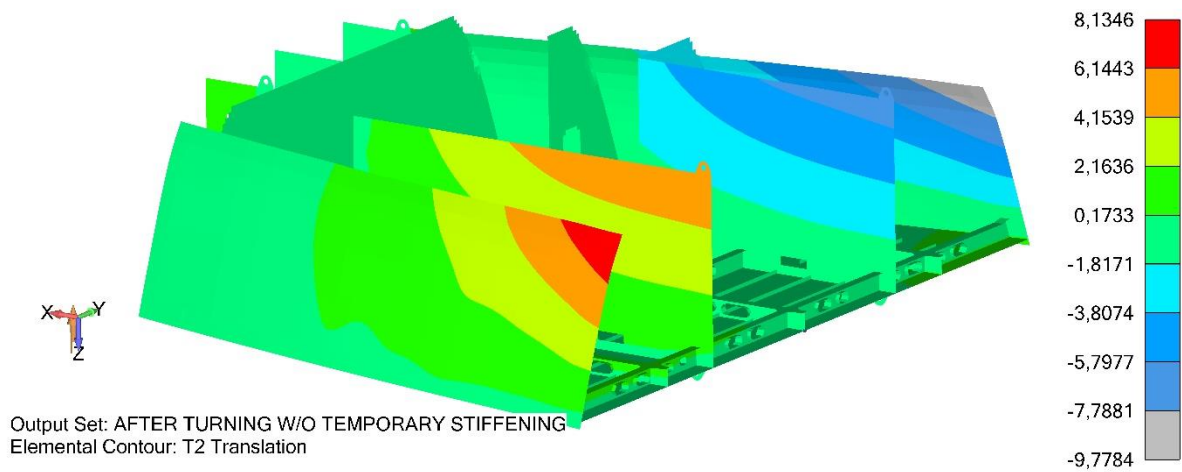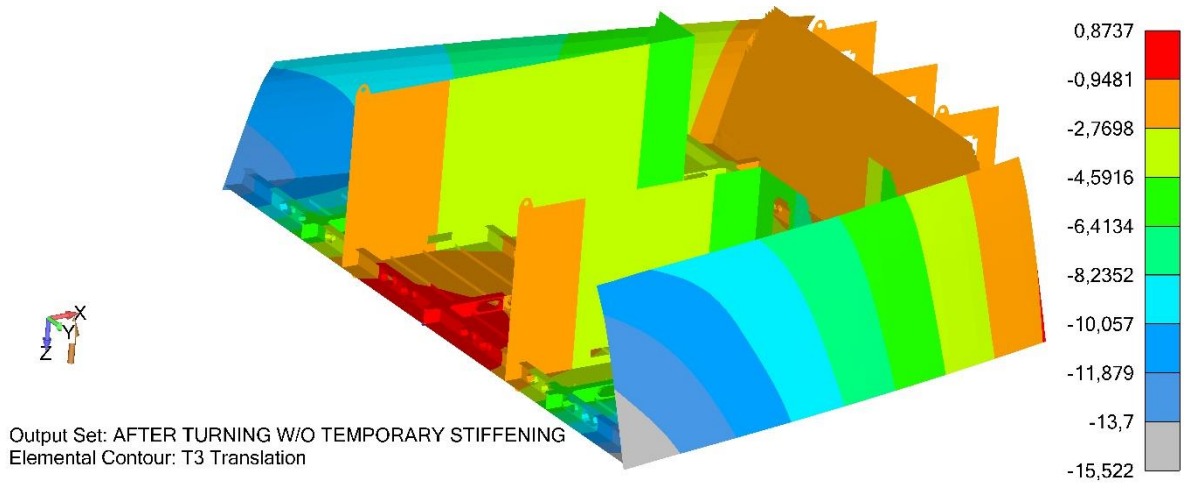Appendix 5. Y - direction translation – turning without temporary stiffening

Appendix 6. Z direction translation – turning without temporary stiffening.

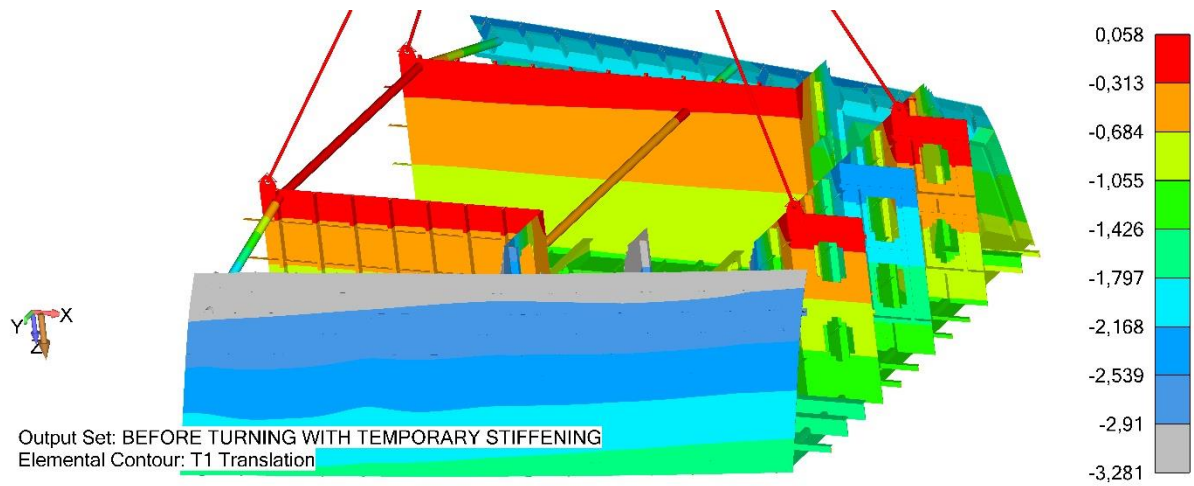Appendix 7. X - direction translation – lifting after turning without temporary stiffening

Appendix 8. Y - direction translation – lifting after turning without temporary stiffening

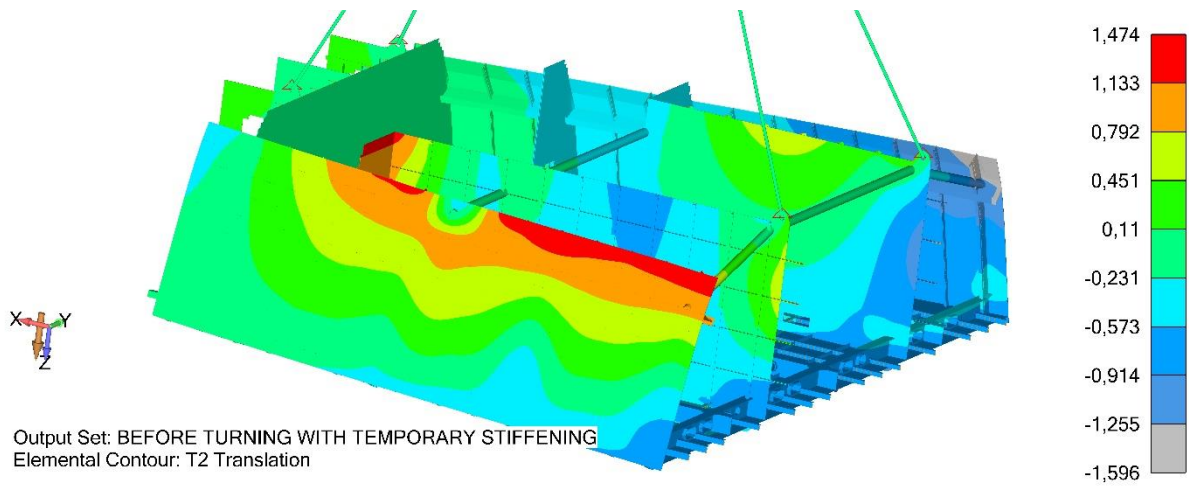Appendix 9. Z - direction translation – lifting after turning without temporary stiffening

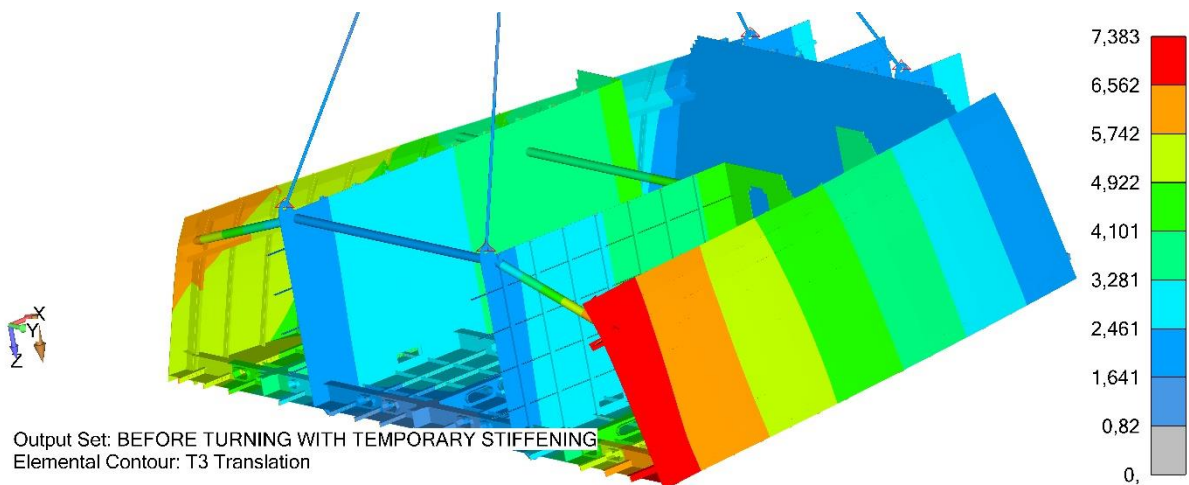Appendix 10. X - direction translation – lifting before turning with temporary stiffening
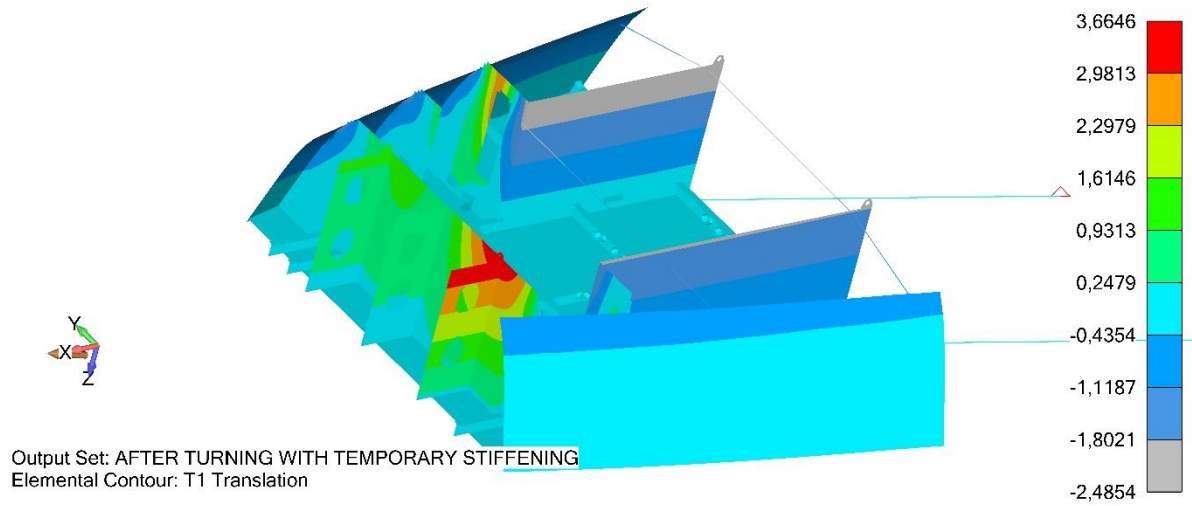
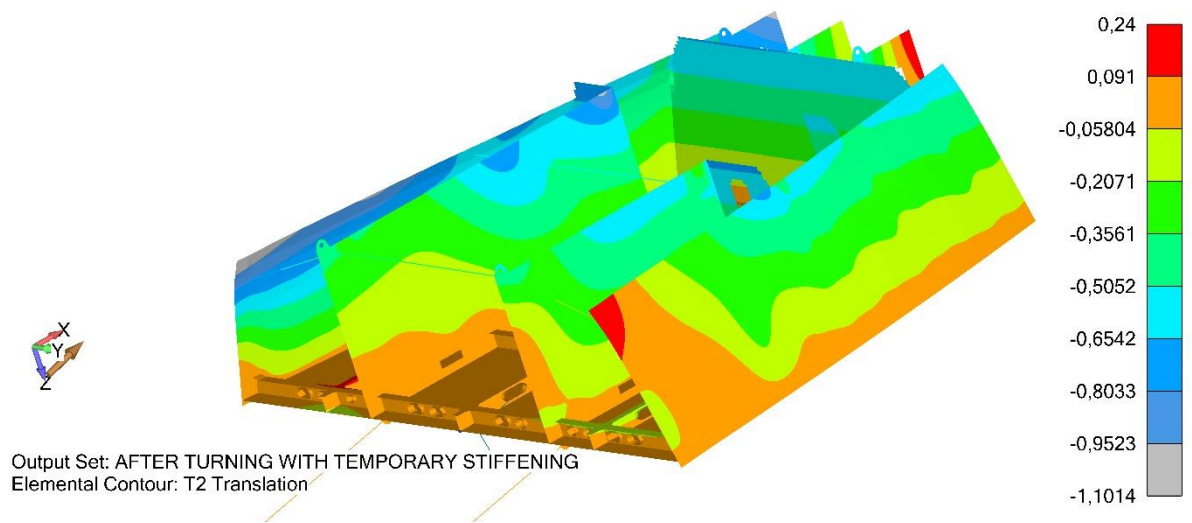Appendix 11. Y- direction translation – lifting before turning with temporary stiffening

Appendix 12. Z - direction translation – lifting before turning with temporary stiffening

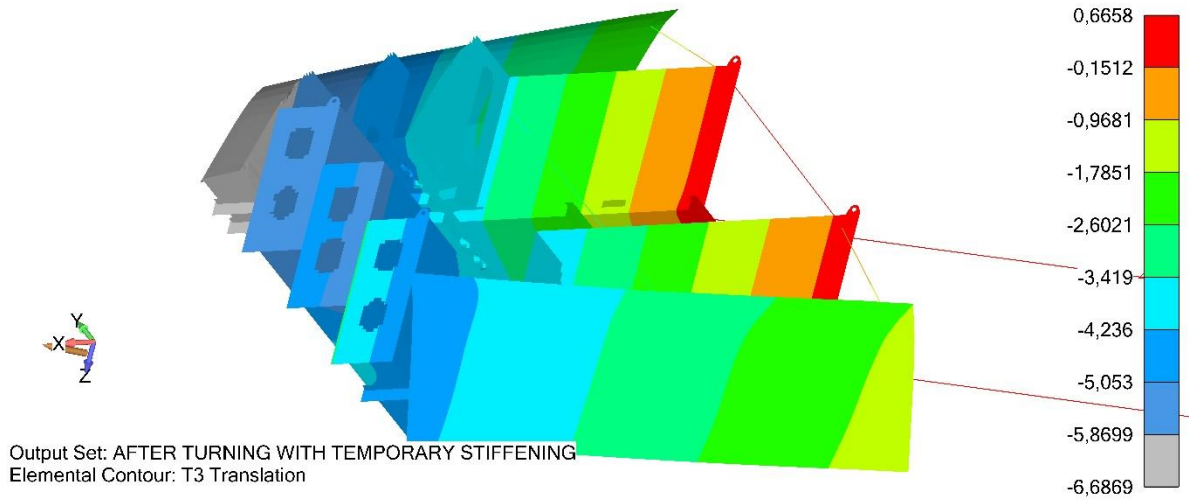Appendix 13. X - direction translation – turning with temporary stiffening.

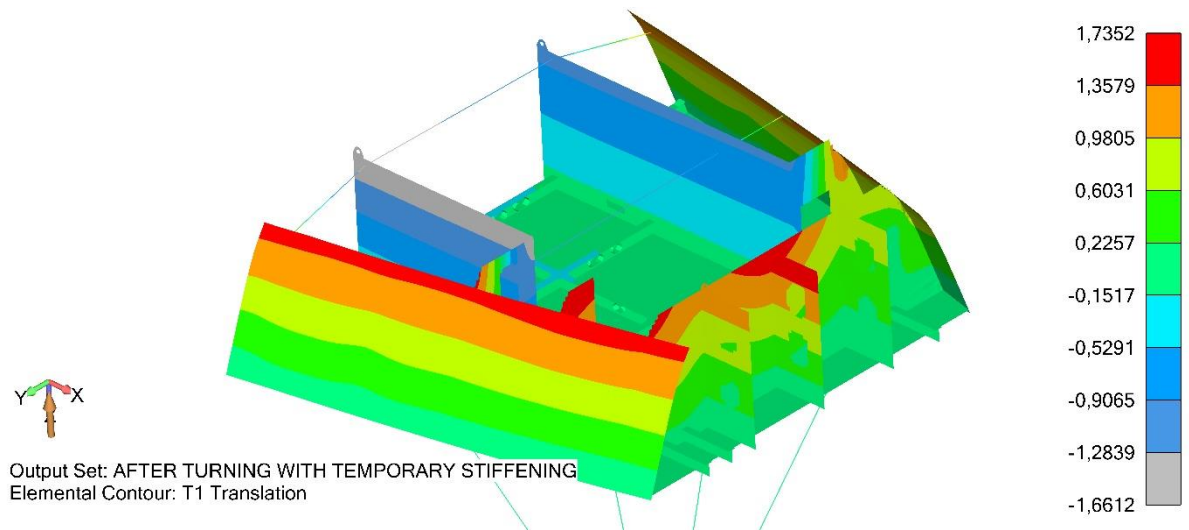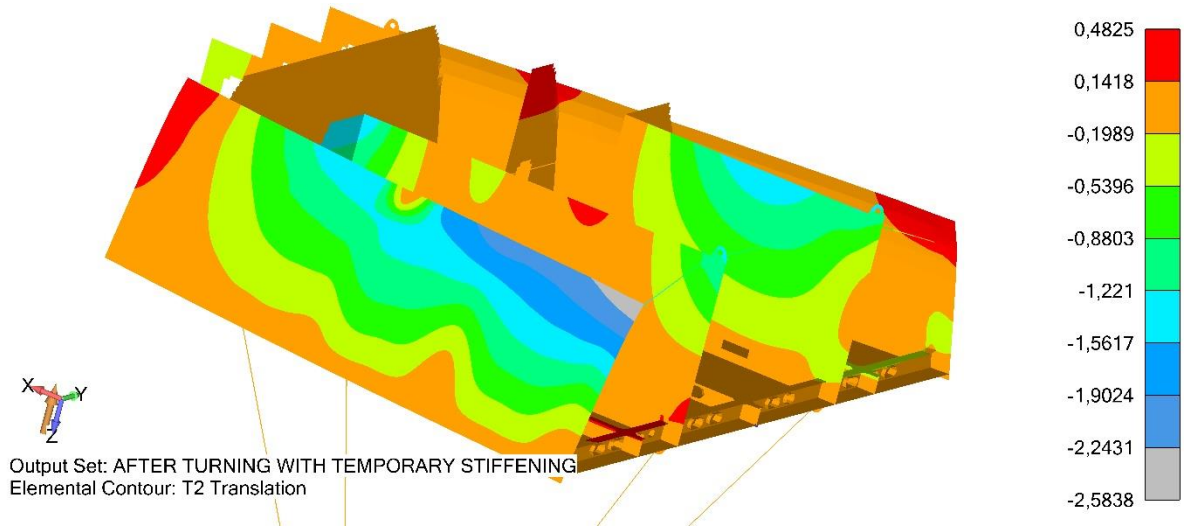Output Set: AFTER TURNING WITH TEMPORARY STIFFENING
Elemental Contour: T1 Translation

Appendix 14. Y - direction translation – turning with temporary stiffening

Output Set: AFTER TURNING WITH TEMPORARY STIFFENING
Elemental Contour: T2 Translation

Appendix 15. Z - direction translation – turning with temporary stiffening

| 0,6658 |
| -0,1512 |
| -0,9681 |
| -1,7851 |
| -2,6021 |
| -3,419 |
| -4,236 |
| -5,053 |
| -5,8699 |
| -6,6869 |

Output Set: AFTER TURNING WITH TEMPORARY STIFFENING
Elemental Contour: T3 Translation

Appendix 16. X - direction translation – lifting after turning with temporary stiffening

| 1,7352 |
| 1,3579 |
| 0,9805 |
| 0,6031 |
| 0,2257 |
| -0,1517 |
| -0,5291 |
| -0,9065 |
| -1,2839 |
| -1,6612 |

Output Set: AFTER TURNING WITH TEMPORARY STIFFENING
Elemental Contour: T1 Translation

Appendix 17. Y - direction translation – lifting after turning with temporary stiffening

Output Set: AFTER TURNING WITH TEMPORARY STIFFENING
Elemental Contour: T2 Translation

Appendix 18. Z - direction translation – lifting after turning with temporary stiffening

Output Set: AFTER TURNING WITH TEMPORARY STIFFENING
Elemental Contour: T3 Translation

Appendix 19. Top views
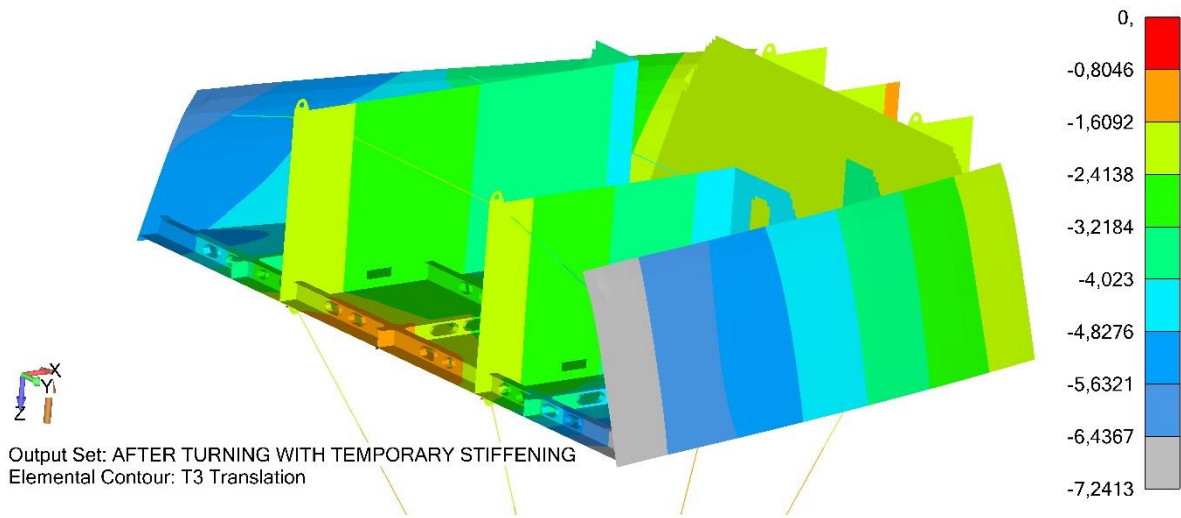
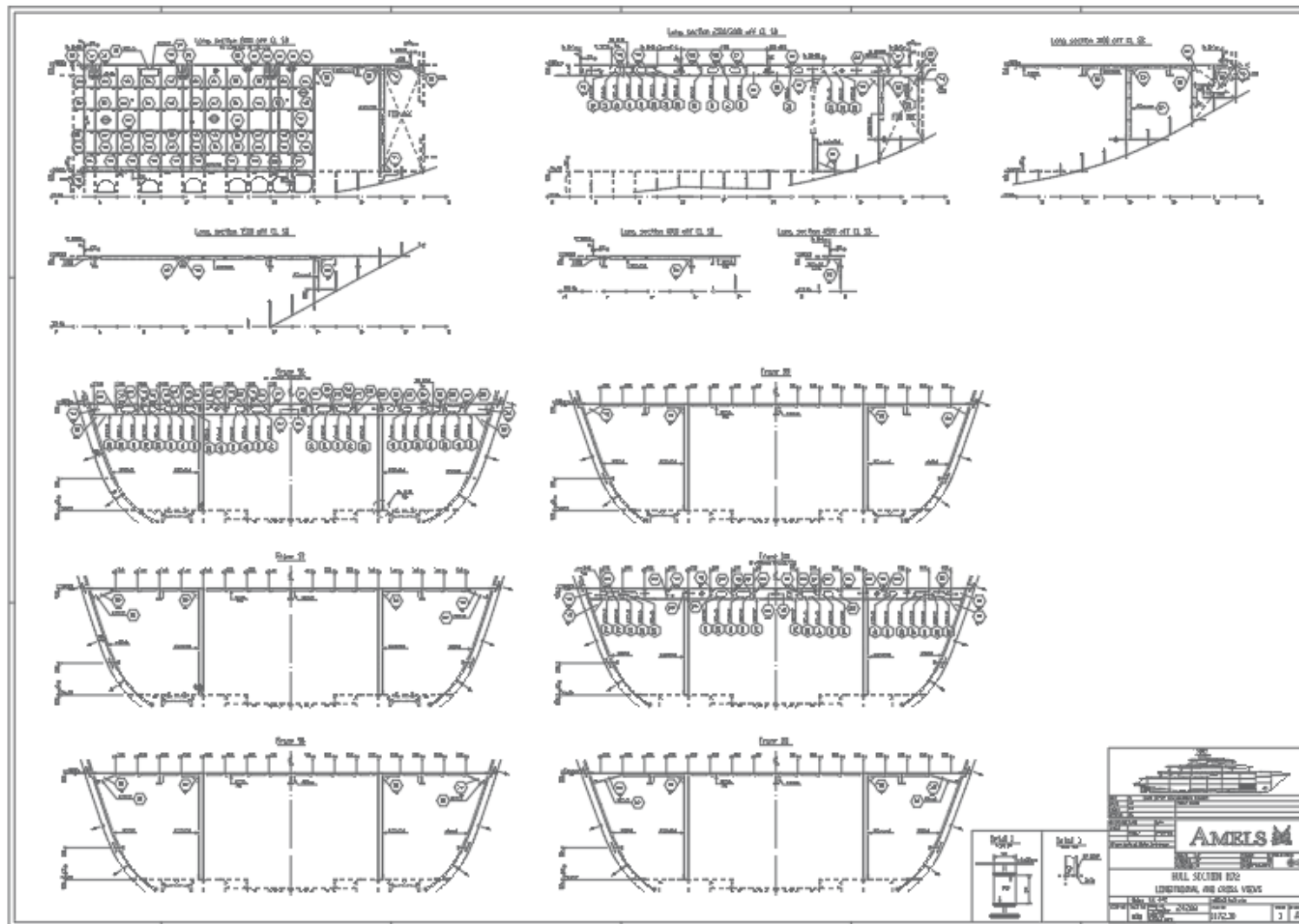## Appendix 20. Longitudinal Views
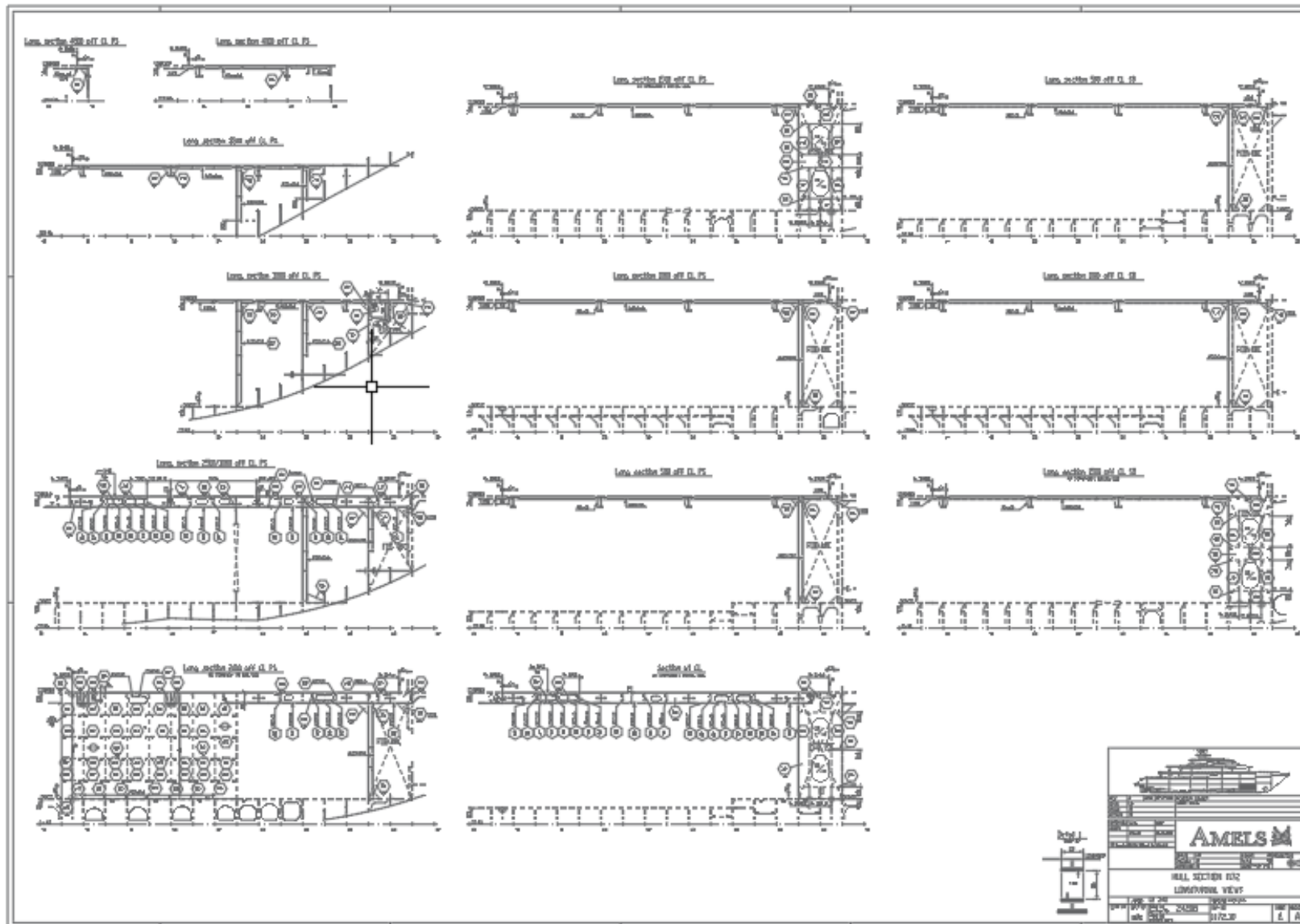
Appendix 21. Longitudinal and cross views

Appendix 22. Cross views

Appendix 23. Lifting plan